

Tumor-agnostic cancer therapy using antibodies targeting oncofetal chondroitin sulfate

Elena Ethel Vidal-Calvo^{1,2*}, Anne Martin-Salazar¹, Swati Choudhary^{1,2}, Robert Dagil^{1,2}, Sai Sundar Rajan Raghavan¹, Lara Duvnjak^{1,2}, Mie Anemone Nordmaj¹, Thomas Mandel Clausen², Ann Skafte^{1,2}, Jan Oberkofler¹, Kaituo Wang³, Mette Ø Agerbaek^{1,4}, Caroline Løppke¹, Amalie Mundt Jørgensen^{1,4}, Daria Ropac¹, Joana Mujollari¹, Shona Willis¹, Agnès Garcias López¹, Rebecca Louise Miller⁵, Richard Torbjörn Gustav Karlsson⁵, Felix Goerdeler⁵, Yen-Hsi Chen⁶, Ana R. Colaço⁷, Yong Wang⁸, Thomas Lavstsen¹, Agnieszka Martowicz⁹, Irina Nelepcu^{10,11}, Mona Marzban^{10,11}, Htoo Zarni Oo^{10,11}, Maj Sofie Ørum-Madsen^{10,11}, Yuzhuo Wang¹⁰, Morten A. Nielsen^{1,2}, Henrik Clausen⁵, Michael Wierer⁷, Dominik Wolf⁹, Ismail Gögenur¹², Thor G. Theander^{1,2}, Nader Al Nakouzi^{2,10,11}, Tobias Gustavsson^{1,2}, Mads Daugaard^{2,10,11*} and Ali Salanti^{1,2*}

¹Centre for Translational Medicine and Parasitology, Department for Immunology and Microbiology, Faculty of Health and Medical Sciences, University of Copenhagen. Copenhagen University Hospital; Copenhagen, Denmark.

²VAR2 Pharmaceuticals ApS; Copenhagen, Denmark.

³Department of Biomedical Sciences, Faculty of Health and Medical Sciences, University of Copenhagen; Copenhagen, Denmark.

⁴VARCT Diagnostics; Copenhagen, Denmark.

⁵Copenhagen Center for Glycomics, Department of Cellular and Molecular Medicine, Faculty of Health and Medical Sciences, University of Copenhagen; Copenhagen, Denmark.

⁶GlycoDisplay ApS; Copenhagen, Denmark.

⁷Proteomics Research Infrastructure, University of Copenhagen; Copenhagen, Denmark.

⁸College of Life Sciences, Zhejiang University; Hangzhou, China.

⁹Department of Internal Medicine V, Haematology & Oncology, Comprehensive Cancer Center Innsbruck (CCCI) and Tyrolean Cancer Research Institute (TKFI), Medical University of Innsbruck; Innsbruck, Austria.

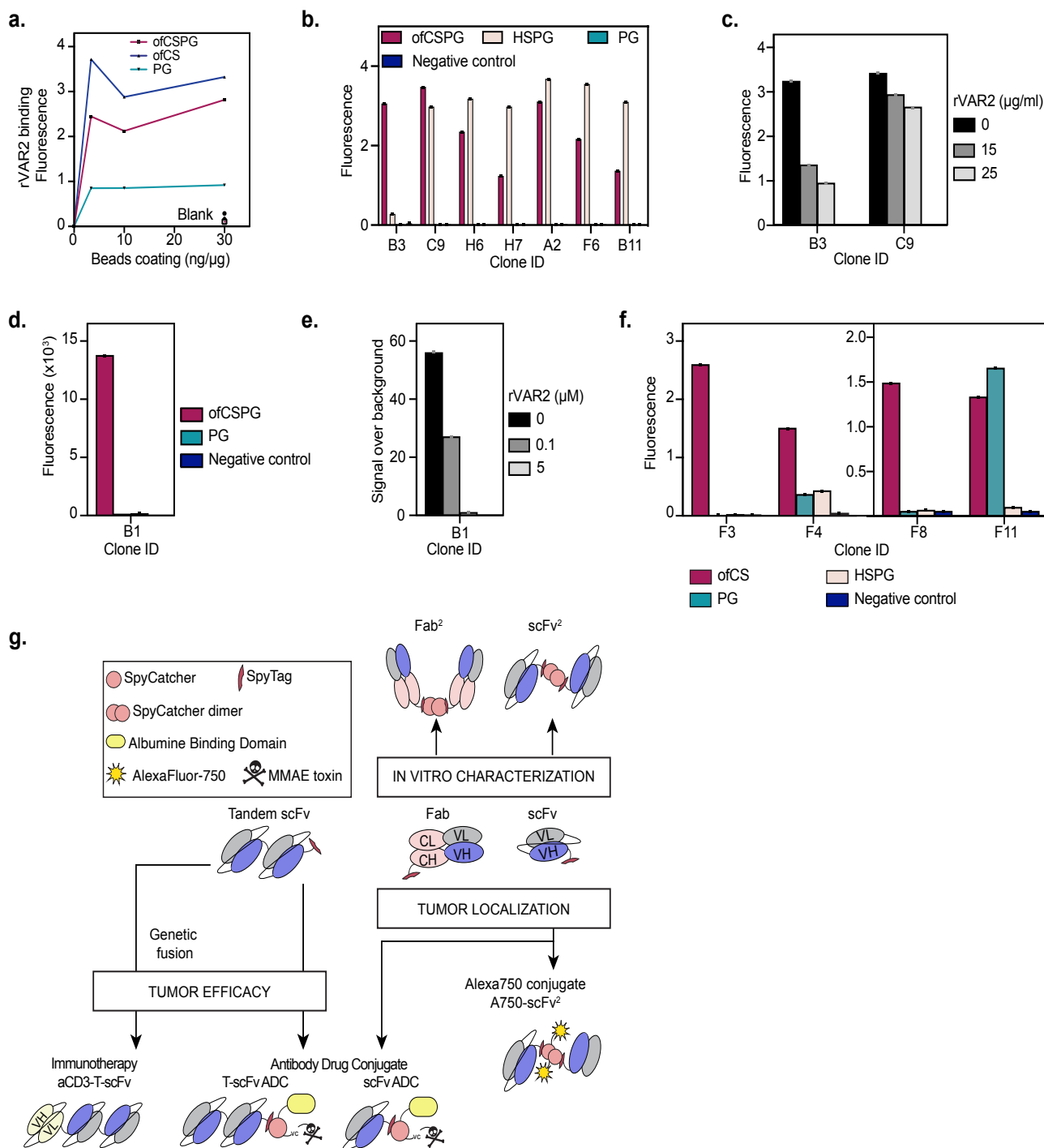
¹⁰Vancouver Prostate Centre, Vancouver Coastal Health Research Institutes; Vancouver, BC, Canada.

¹¹Department of Urologic Sciences, Faculty of Medicine, University of British Columbia; Vancouver, BC, Canada.

¹²Center for Surgical Science, Department of Surgery, Zealand University Hospital Køge; Køge, Denmark.

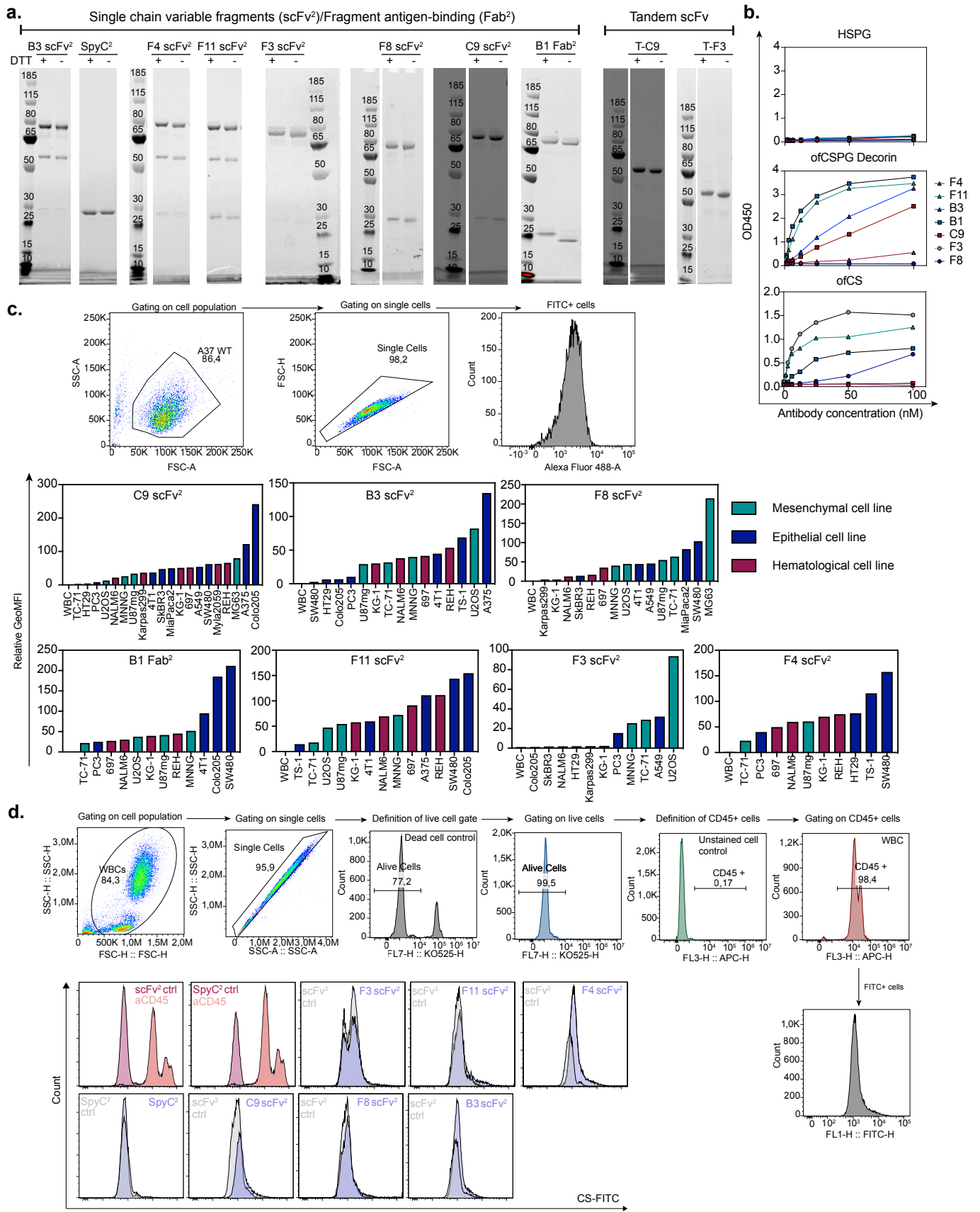
*Corresponding authors. Emails: elena@sund.ku.dk; mads.daugaard@ubc.ca; salanti@sund.ku.dk

Supplementary Fig. 1: Identification of CS specific phage-derived antibody fragments.



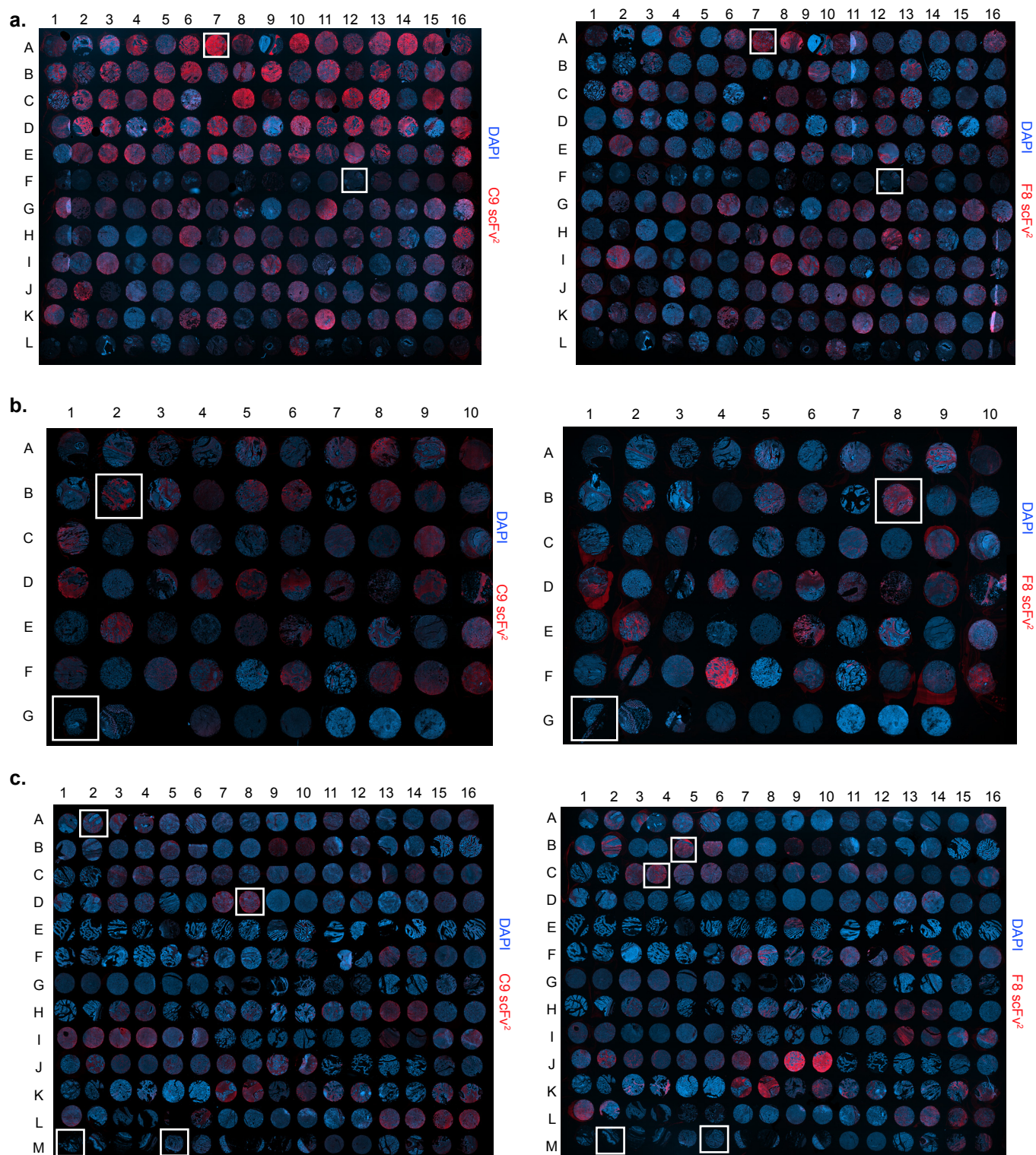
a. Resulting fluorescence signals (OD450) of V5-tagged rVAR2 binding to increasing amounts of biotinylated ofCSPG, PG and ofCS immobilized on streptavidin-blocked-coated beads and detected with anti-V5 HRP. Controls consisted of coated beads without addition of rVAR2 and rVAR2 binding to naked bead (blank on the figure). **b.** Monoclonal ELISA results of B3, C9 and the clones discarded from the study (H6, H7, A2, F6, B11), identified from the LiAb-SFMAXTM library, to ofCSPG, PG and HSPG (n=1 sample per condition). **c.** ELISA results of B3 and C9 clones binding to ofCSPG where the binding was competed with increasing concentrations of rVAR2 protein, as indicated (n=1 sample per condition). **d.** Monoclonal ELISA results of B1 clone binding, identified from the HuCal library, to ofCSPG and PG and BSA (negative control) (n=1 sample per condition). **e.** ELISA results of B1 clone as in **c.** (n=1 sample per condition). **f.** Monoclonal ELISA binding results of F3, F4, F8 and F11 clones, identified from Althea library, to ofCS, ofCSPG, PG and HSPG (n=1 sample per condition). **g.** Schematic representation of antibody formats produced for *in vitro* characterization, *in vivo* tumor localization and anti-tumor efficacy studies using SpyT-SpyC click conjugation. Source data are provided as a Source Data file.

Supplementary Fig. 2: Phage derived antibody fragments bind to a vast range of human cancer cells with limited binding to white blood cells.



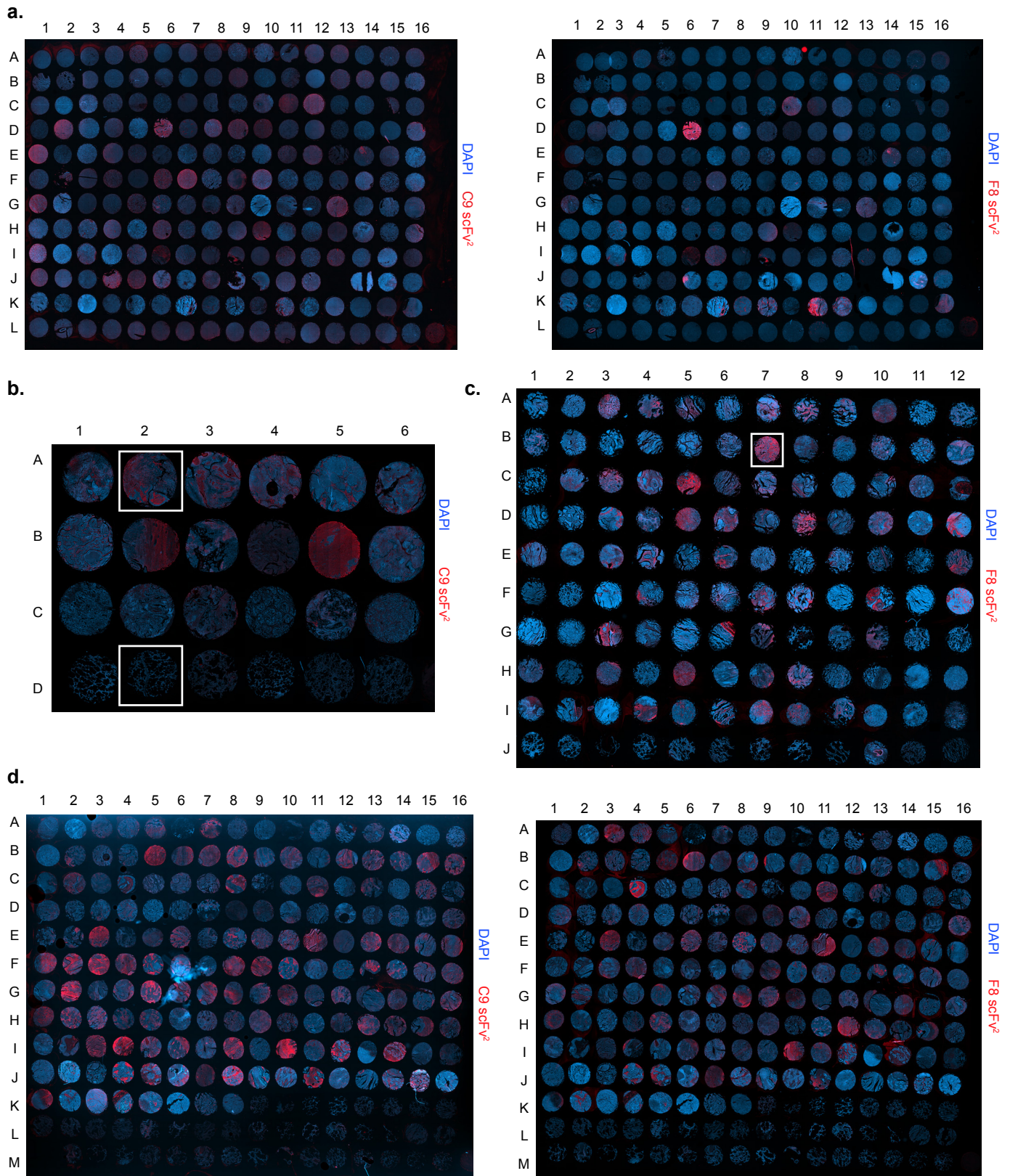
a. SDS PAGE of antibody fragments (scFv², Fab²) used for *in vitro* characterization, treated with dithiothreitol (DTT+) prior to loading. **b.** Optical density (OD450) of [0-100]nM V5-scFv² (F3, F4, F8, F11, C9, B3) or FLAG-Fab² (B1) binding to commercialized HSPG, recombinant ofCSPG and purified ofCS (n=1 sample per condition). **c.** Relative Geometric Mean Intensity (GeomFI) of 150nM V5-tagged-scFv² (F3, F4, F8, F11, C9, B3) or FLAG-tagged-Fab² (B1) binding to purified human white blood cells or cancer cells from different origin (mesenchymal (green), epithelial (blue), and hematological (red)) and detected with FITC-anti tag antibodies, with exemplified gating strategy. (n=1 sample per condition) **d.** Representative histograms of binding intensities to purified human white blood cells stained with anti-CD45 and 300nM V5-tagged-scFv² (F3, F11, F4, C9, F8 and B3) or SpyC2 protein control, with exemplified gating strategy. Source data are provided as a Source Data file.

Supplementary Fig. 3: C9 and F8 discriminate malignant from healthy tissues from breast and the digestive system.



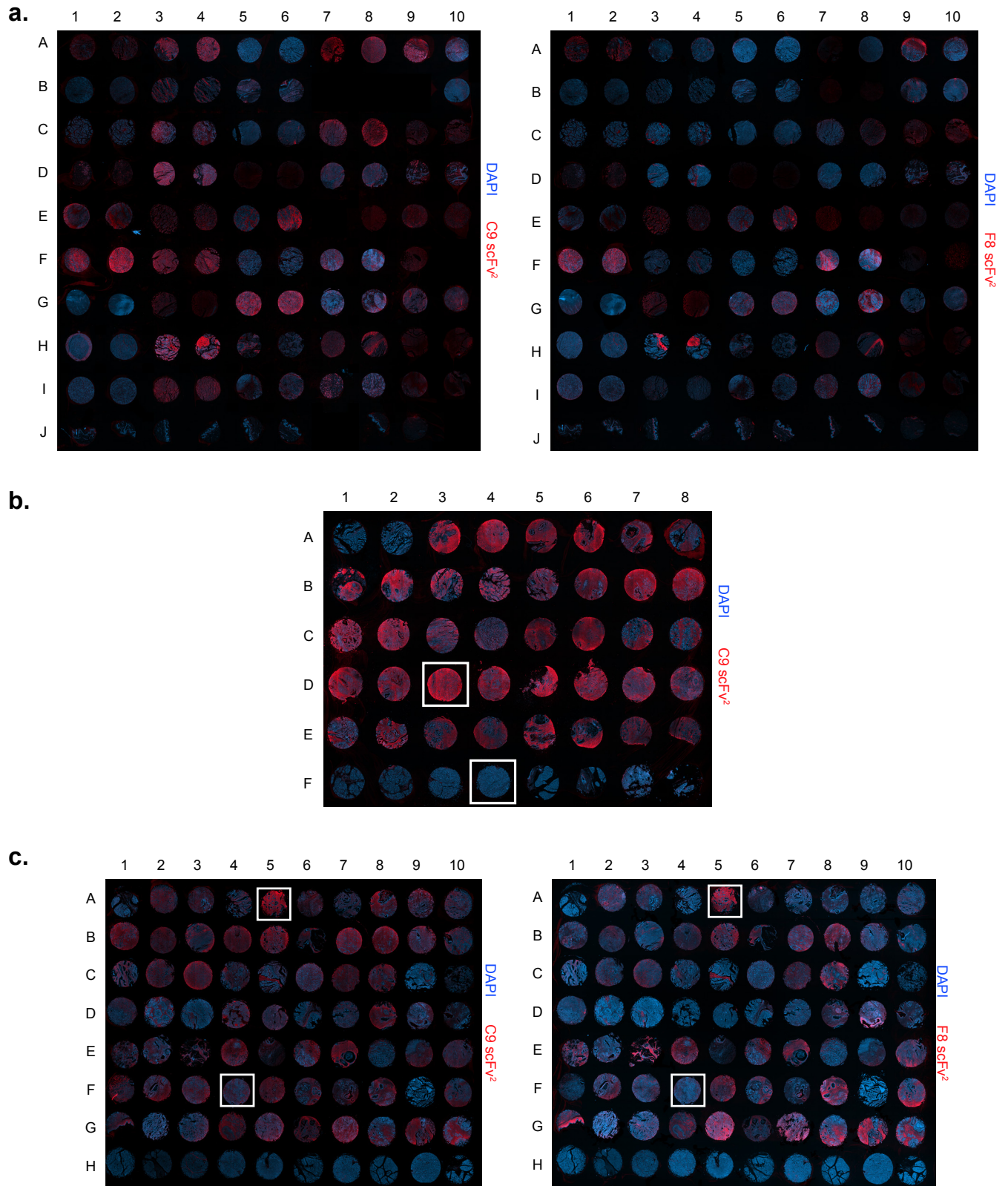
a. Immunofluorescence scans of a breast cancer tissue array (BR1921c) stained with 25nM C9 or F8 scFv² (red) while cell nuclei are stained with DAPI (blue). **b.** Immunofluorescence scans of a colon primary cancer tissue array with metastatic tissues (CO702) stained as in **a.** **c.** Immunofluorescence scans of an array containing tissues from the digestive system (DGS2081) stained as in **a.** The sections encircled in white are used in the panel Fig. 2b.

Supplementary Fig. 4: C9 and F8 discriminate malignant from healthy tissues from brain and lung.



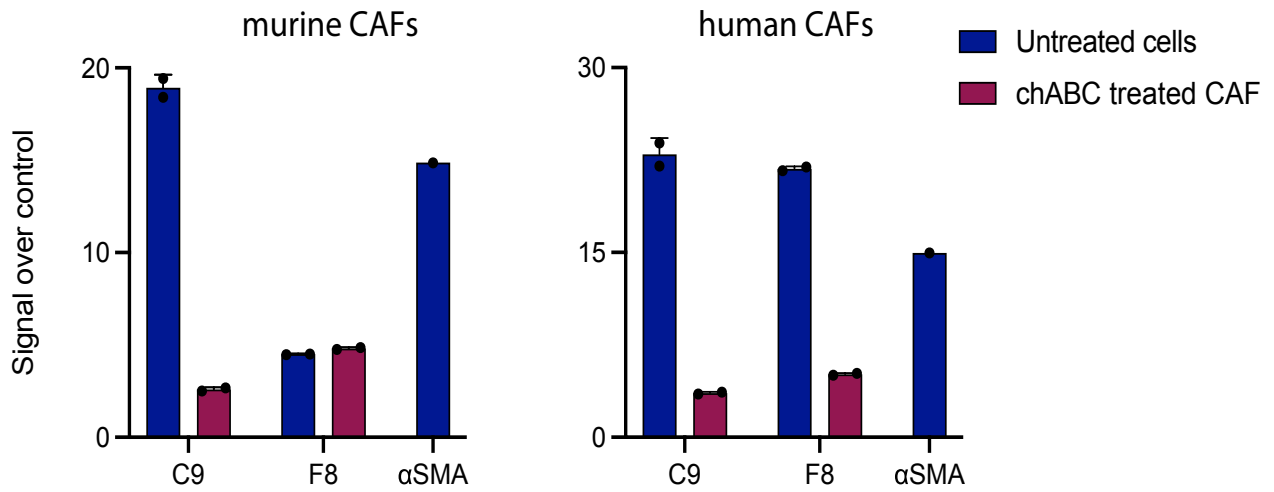
a. Immunofluorescence scans of a brain cancer tissue array (GL2083) stained with 25nM C9 or F8 scFv² (red) while cell nuclei are stained with DAPI (blue) **b.** Immunofluorescence scans of a lung cancer tissue array (LC243a) stained with C9 as in **a.** **c.** Immunofluorescence scans of a lung cancer tissue array (LC1201b) stained with F8 as in **a.** **d.** Immunofluorescence scans of a lung cancer tissue array (LC2085d) stained as in **a.** The sections encircled in white are used in the panel Fig. 2b.

Supplementary Fig. 5: C9 and F8 discriminate malignant from healthy tissues from skin and pancreas.



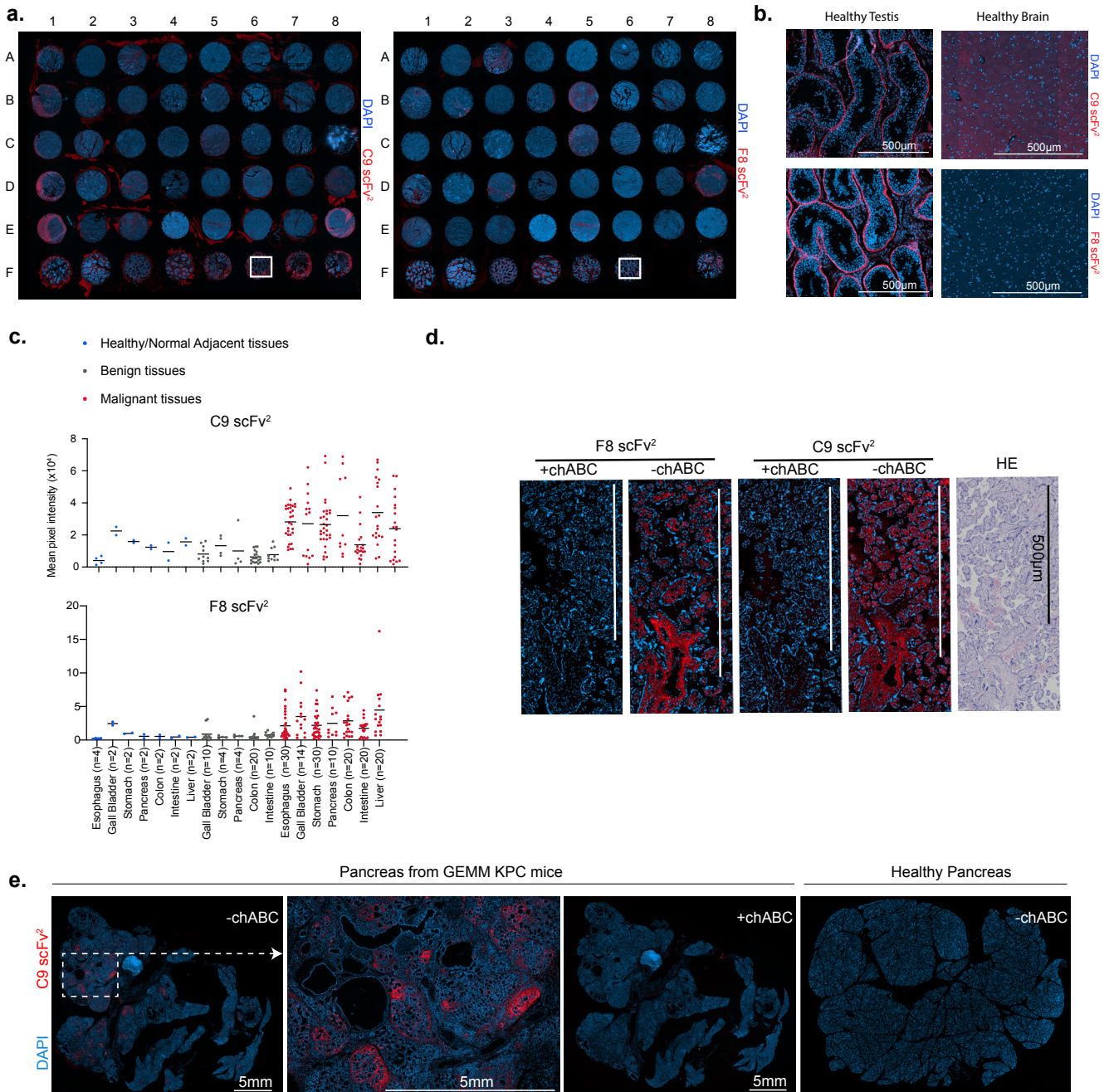
a. Immunofluorescence scans of a melanoma and skin tissue array (ME1002b) stained with 25nM C9 or F8 scFv² (red) while cell nuclei are stained with DAPI (blue). **b.** Immunofluorescence scans of a PDAC array (PA482) stained with C9 as in **a.** **c.** Immunofluorescence scans of a pancreatic cancer array (PA804b) stained as in **a.** The sections encircled in white are used in panel Fig. 2b.

Supplementary Fig. 6: Reactivity of C9 and F8 antibody fragments to cancer-associated fibroblasts (CAF).



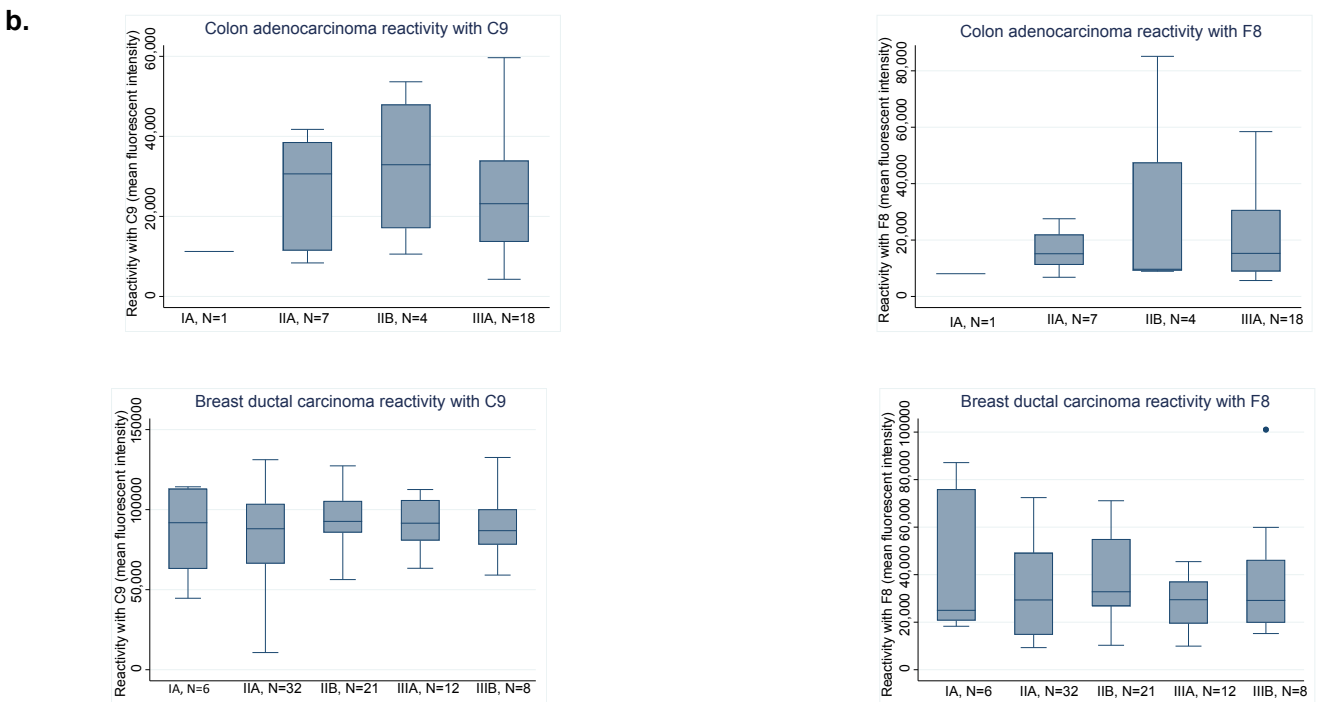
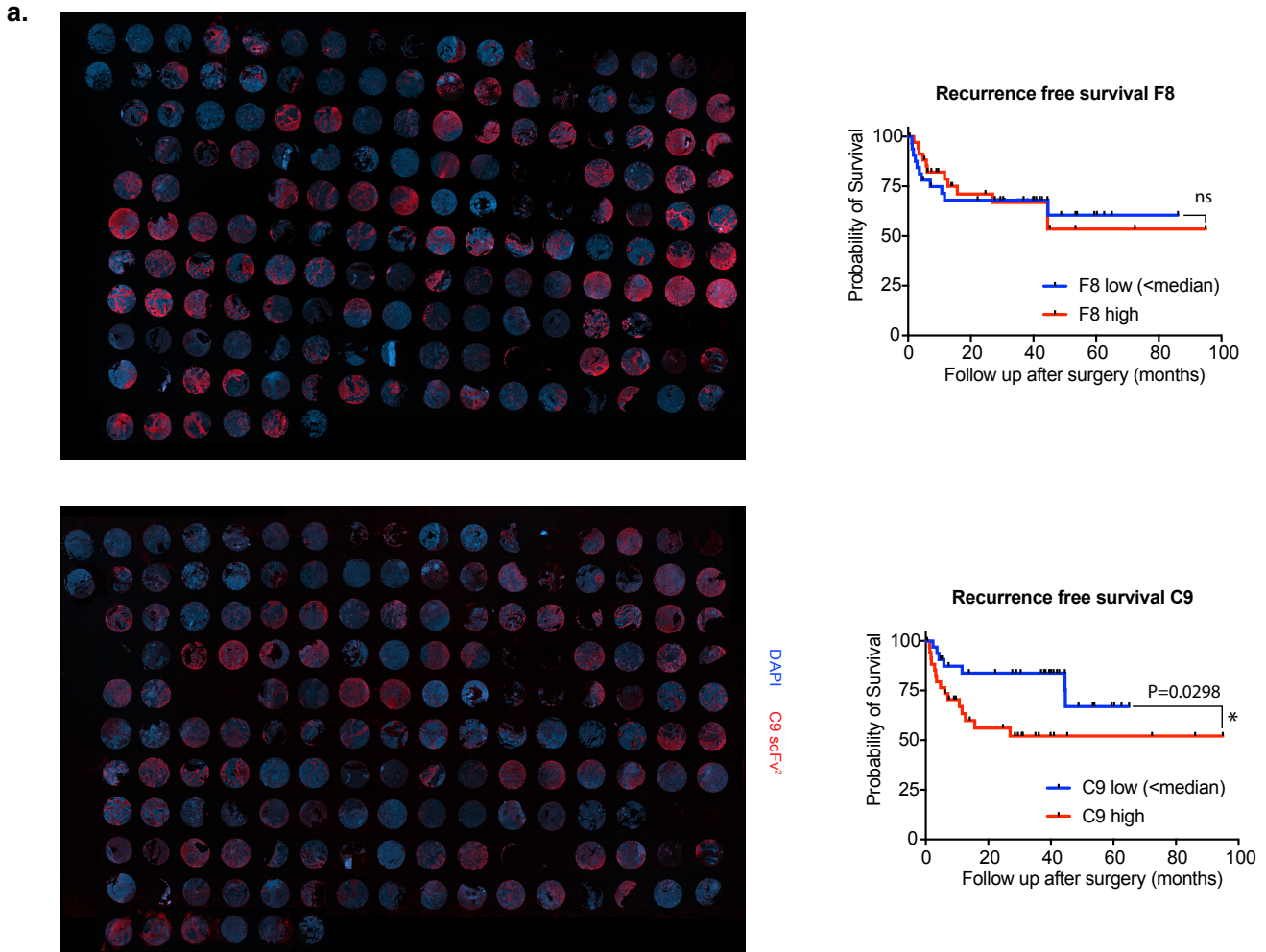
Resulting mean fluorescence intensity normalized over control of C9 and F8 scFv² and αSMA staining, detected with Anti-V5-FITC and anti-Rabbit-Alexa647 antibodies, respectively, of human (vCAF) and murine (mCAF) cancer-associated fibroblast (CAF) (n=2 samples per condition). Error bars represent standard error of the mean. Source data are provided as a Source Data file.

Supplementary Fig. 7: C9 and F8 bind to onco-fetal CS epitope with limited off-target binding.



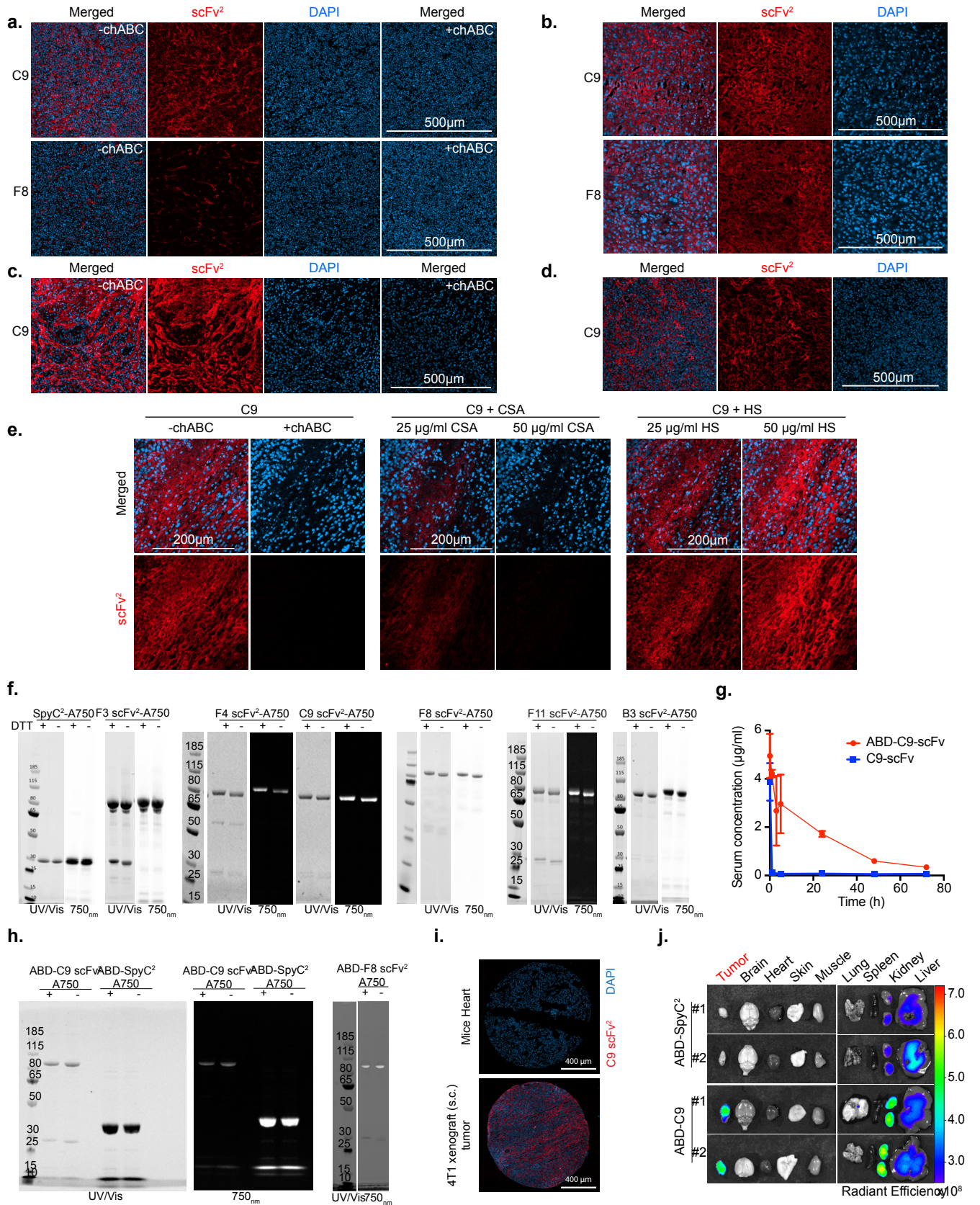
a. Immunofluorescence scans of a testis tissue array (TE481a) stained with 25nM C9 or F8 scFv² (red) with cell nuclei stained with DAPI (blue). The sections encircled in white are used in Supplementary Fig. 7b. **b.** Healthy testis (TE481a) and brain (GL2083) tissues stained as in **a.** **c.** Mean pixel intensity of DGS2081 stained as described in **a.** where each dot represents a tissue section with number of sections (n) indicated for each group. Intensities were measured on Fiji software. **d.** Hematoxylin and Eosin (HE) and immunofluorescence staining of human placenta stained as described in **a.** with or without chABC treatment. **e.** Immunofluorescence staining of pancreas from KPC or healthy Balb/c mice stained in combination with chABC treatment as indicated, stained with C9 as in **a.** Source data are provided as a Source Data file.

Supplementary Fig. 8: Abundance of C9 epitope correlates with poor survival in bladder cancer.



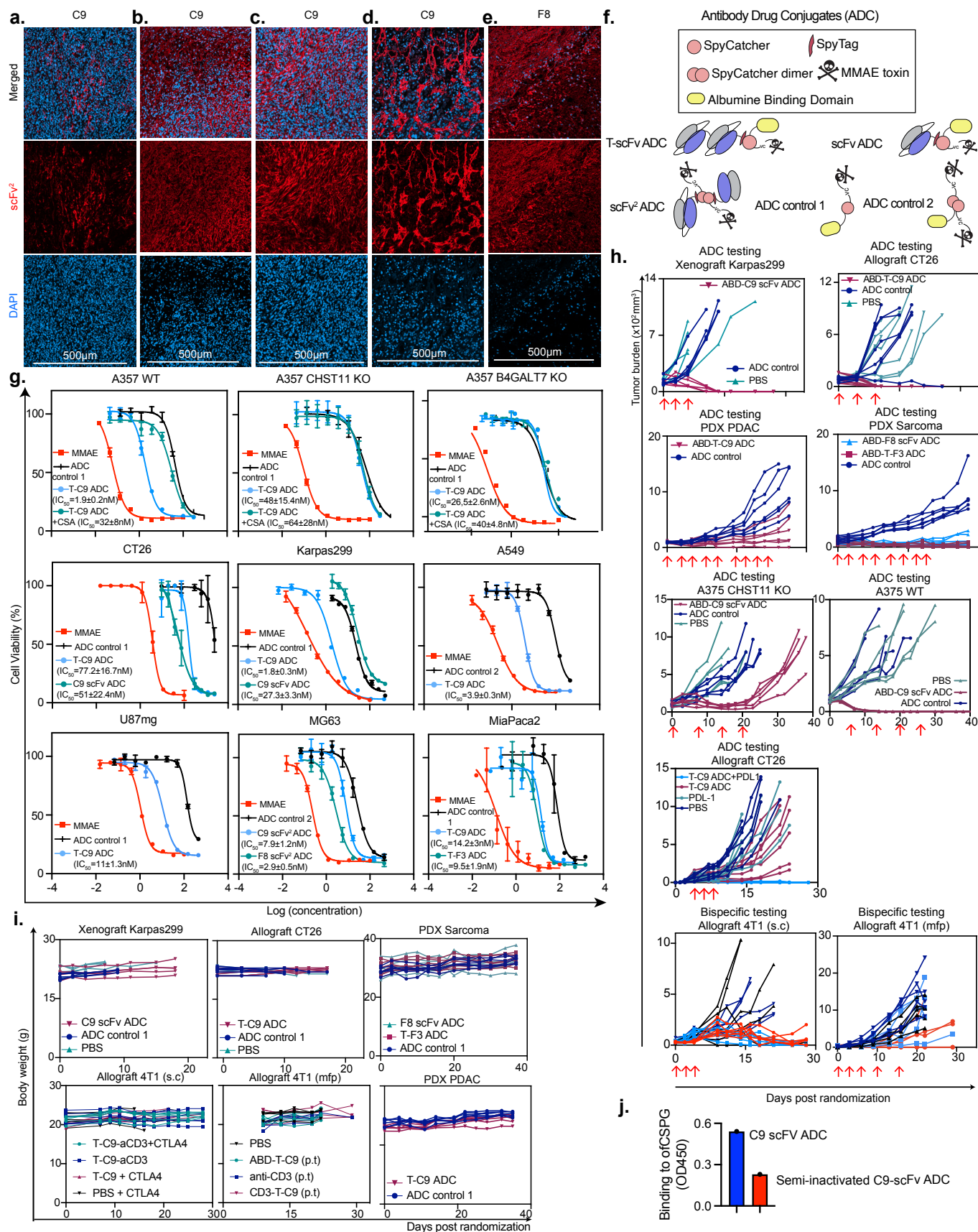
a. Immunofluorescence scans of a bladder cancer tissue array stained with 25nM C9 or F8 scFv² (red) with cell nuclei stained with DAPI (blue). Staining intensity of each tissue core was correlated with patient's survival. **b.** Mean pixel intensity of colon adenocarcinoma (CO702d) and breast ductal carcinoma (BR1921c) reactivities with F8 and C9 correlated to stages with standard deviation as error bars. Source data are provided as a Source Data file.

Supplementary Fig. 9 Anti-ofCS C9 antibody localizes in ofCS-expressing tumor *in vivo*.



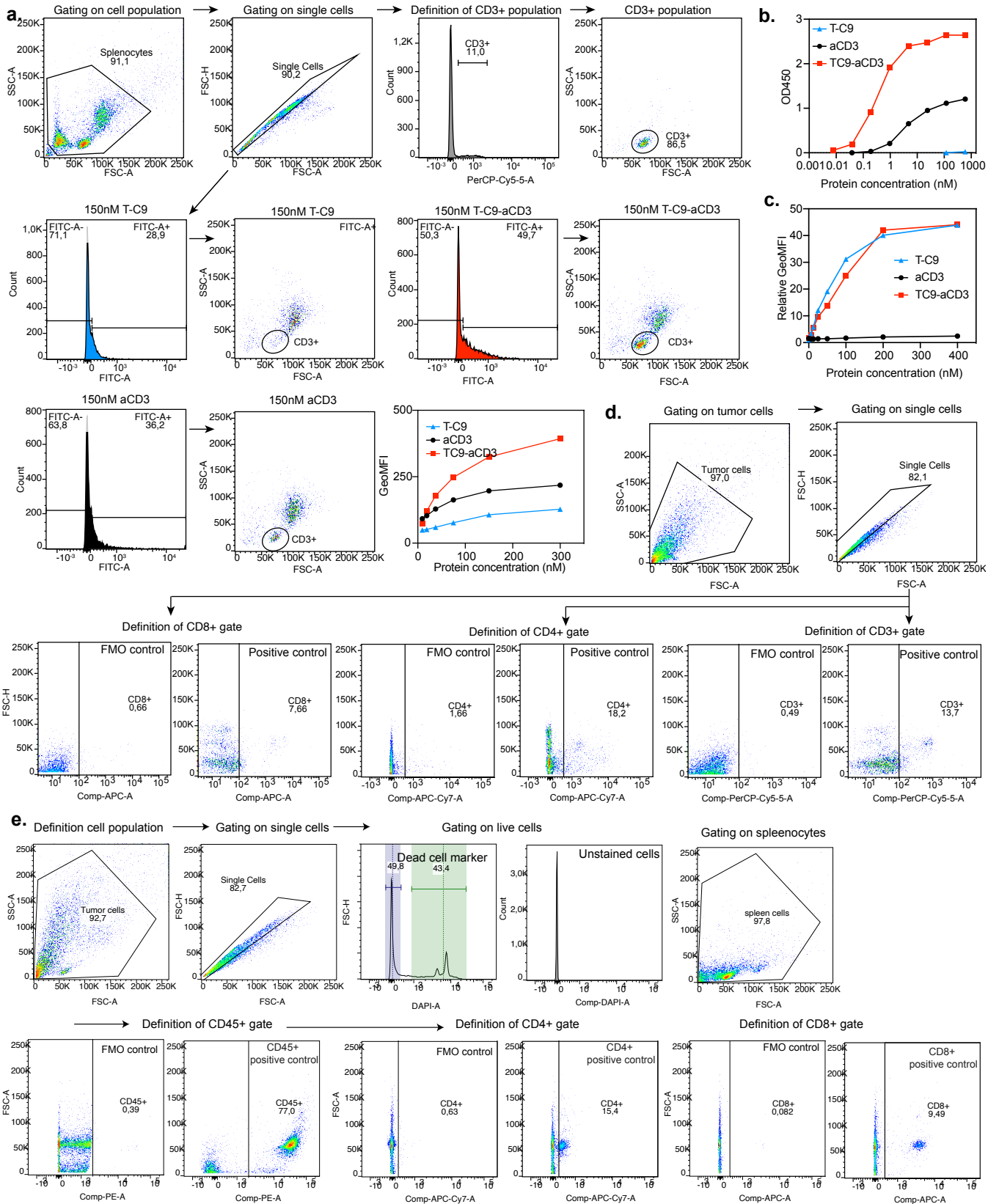
a. Karpas299 tumors stained with 25nM C9 and F8 scFv² detected with Anti-V5-Alexa647 (red), with (+chABC) or without (-chABC) chABC treatment (chABC), and nuclei in blue (DAPI). **b.** Neuroendocrine prostate Patient derived xenograft (PDX). **c.** A549 and **d.** MiaPaca2 tumor tissues, stained as in **a.** **e.** Karpas299 tumors stained with C9 as in **a.** where binding was inhibited with soluble CSA or HS at indicated concentrations. **f.** SDS PAGE of Alexa750 conjugated scFv² and **g.** Serum concentration of injected proteins of rats (n=2) injected with 100 µg C9 scFv or ABD-C9-scFv. **h.** ABD-scFv² used for *in vivo* IVIS studies, treated with dithiothreitol (DTT) as indicated, prior to loading 1 µg of protein per well. **i.** Immunofluorescence staining of healthy heart, and xenograft 4T1 tumor stained as in **a.** **j.** Ex vivo scanning of A549 lung xenograft model 24h after injection of 50 µg of indicated proteins. Source data is provided in a Source data file.

Supplementary Fig. 10: Anti-ofCS antibodies elicit anti-tumor efficacy *in vivo* as antibody drug conjugates.



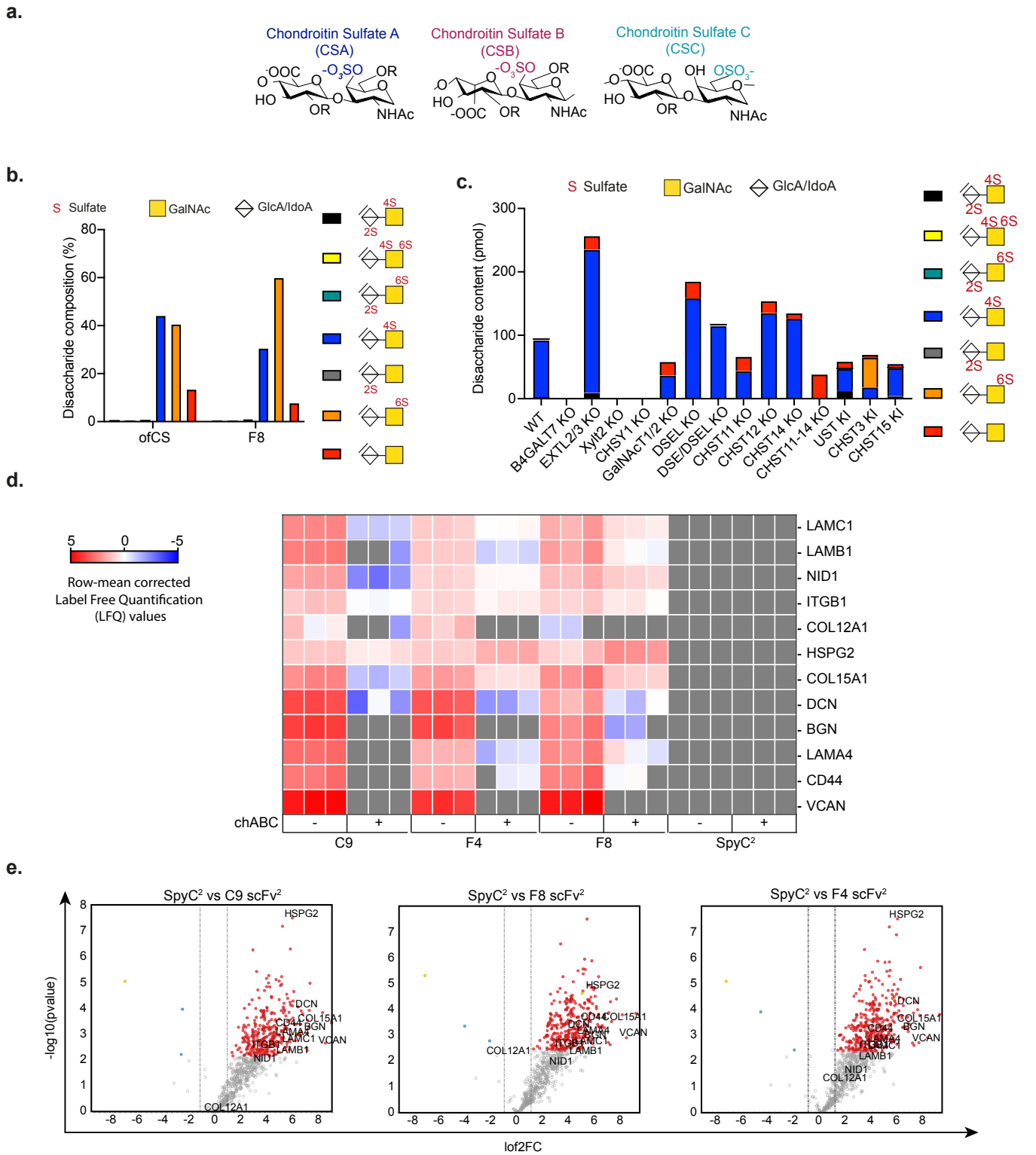
a. CT26, **b.** 4T1 (s.c.), **c.** 4T1 (mfp), **d.** PDX PDAC, **e.** PDX Sarcoma tissues stained with 25nM scFv² as indicated, detected with Anti-V5-Alexa647 (red) with cell nuclei in blue (DAPI). **f.** Schematic representation of constructs used in **g.** **g.** Cytotoxicity of indicated proteins incubated with indicated cell lines at [0-2400] nM concentrations (n=3 samples per condition). **h.** Individual tumor burden (mm³) and **i.** body weight of mice for each indicated treatment group and studies. Red arrows indicate days of treatment. **j.** Optical density (OD450) of 200nM C9-scFv ADC (blue) and semi-inactivated C9-scFv ADC (red) binding to commercialized ofCSPG (aggrecan) (n=1 per condition). Source data are provided as a Source Data file.

Supplementary Fig. 11: Anti-ofCS bispecific and ADC recruit immune cells in the tumor microenvironment.



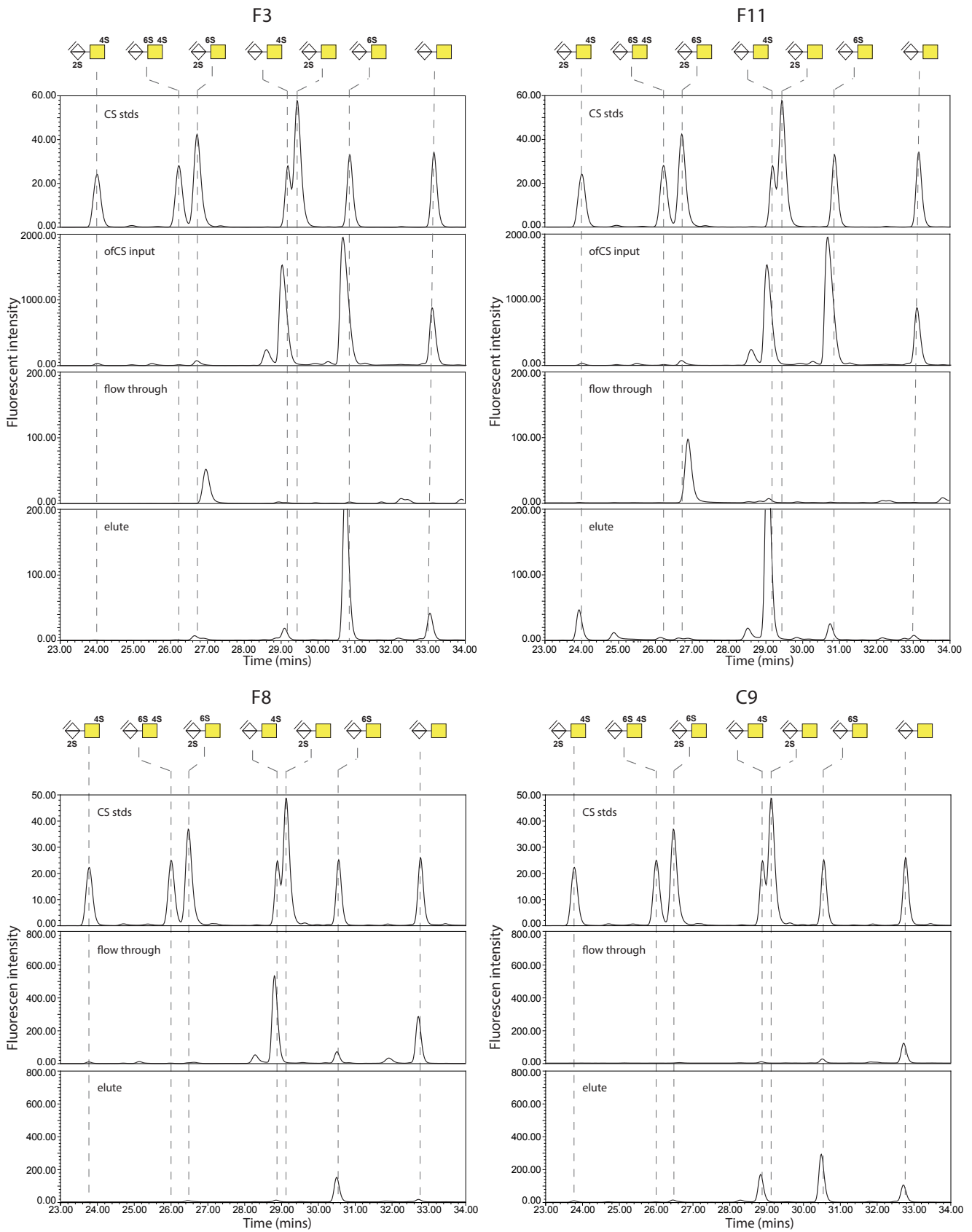
a. Resulting binding of 150nM anti-CD3, T-C9, aCD3-T9 proteins to fresh splenocytes in flow cytometry, with a focus on CD3+ cell population. **b.** Optical Density (OD450) of T-C9-aCD3, aCD3 and T-C9 binding to recombinant murine aCD3 protein tested for [0.01-600]nM concentration. **c.** Relative GeomFI intensity of V5-tagged T-C9-aCD3, aCD3 and T-C9 binding to 4T1 cancer cells in flow cytometry was tested for [0-400]nM concentration. **d.** Gating strategy for counting immune cells (CD3+, CD8+ and CD4+) in 4T1 mfp tumors suspensions (n=2) after three treatments with PBS, aCD3 or T-C9-aCD3. **e.** Gating strategy for counting immune cells (CD45+, CD8+ and CD4+) in CT26 tumors suspensions (n=2 or 3) after three treatments with T-C9 ADC alone or in combination with PDL1, compared to PDL-1 and PBS controls.

Supplementary Fig. 12: Antibody fragments bind to Chondroitin sulfate chains onto proteoglycans.



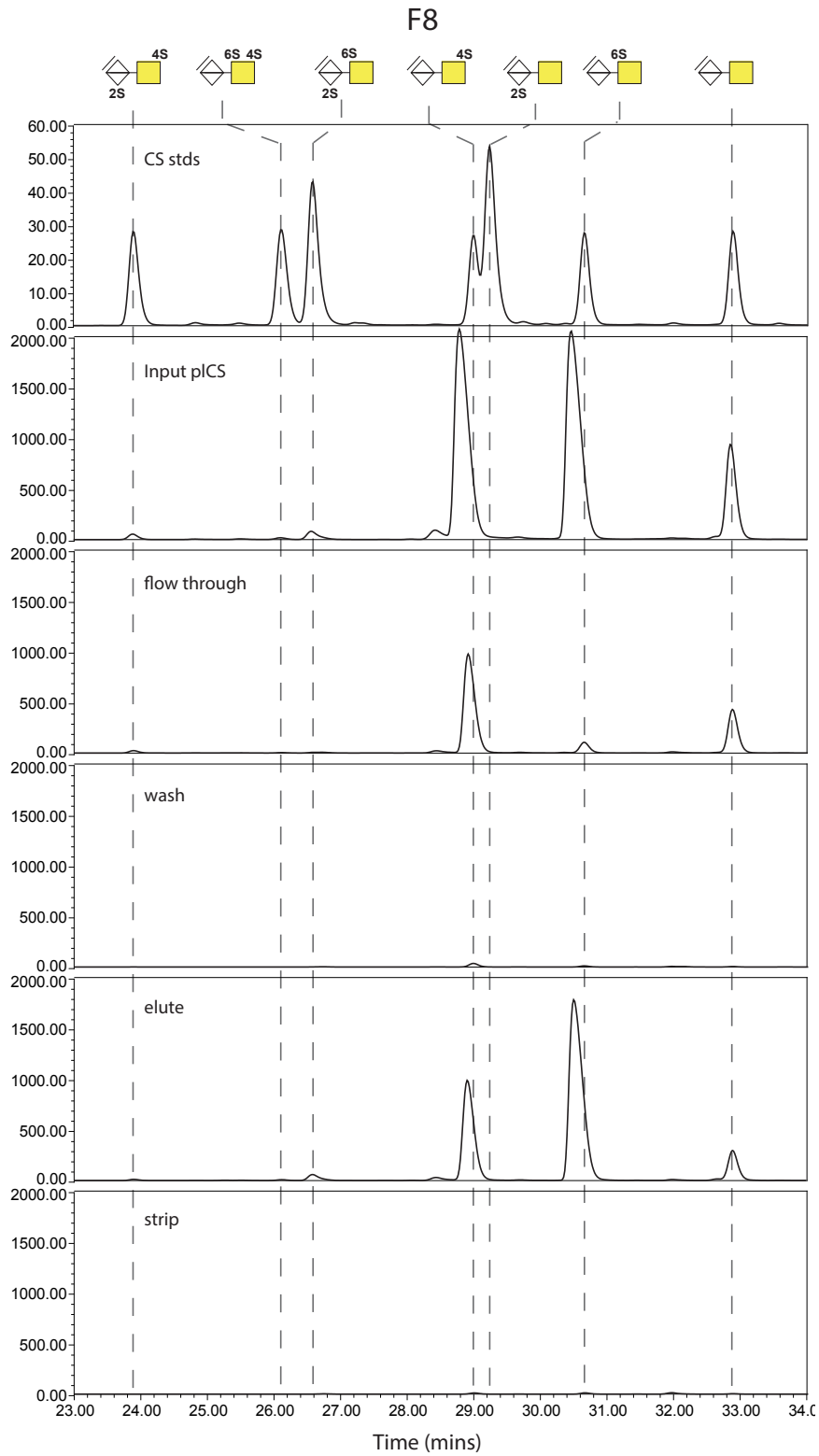
a. Chair conformations of chondroitin sulfate A, B and C molecules. **b.** Full chain analysis of ofCS pull-downs with F8 scFv² performed by disaccharide analysis. (n=1 sample per condition) **c.** Disaccharide analysis of GAG KO/KI engineered CHO cell lines (n=1 sample per condition). **d.** Heatmap representing row mean corrected label-free quantification (LFQ) values of hits obtained by MS analysis of CSPG pull-downs from a human colon biopsy (H386) with C9, F4 and F8 scFv² and SpyC², in combination with chABC treatment as indicated, prior to enrichment, with imputed values removed and colored in grey. **e.** Volcano plot of human colon biopsy (H386) processed and analyzed in **d.** with selected CSPG hits highlighted in black for each protein. Source data are provided as a Source Data file.

Supplementary Fig. 13: Foot-print analysis of antibody fragments' binding epitopes.



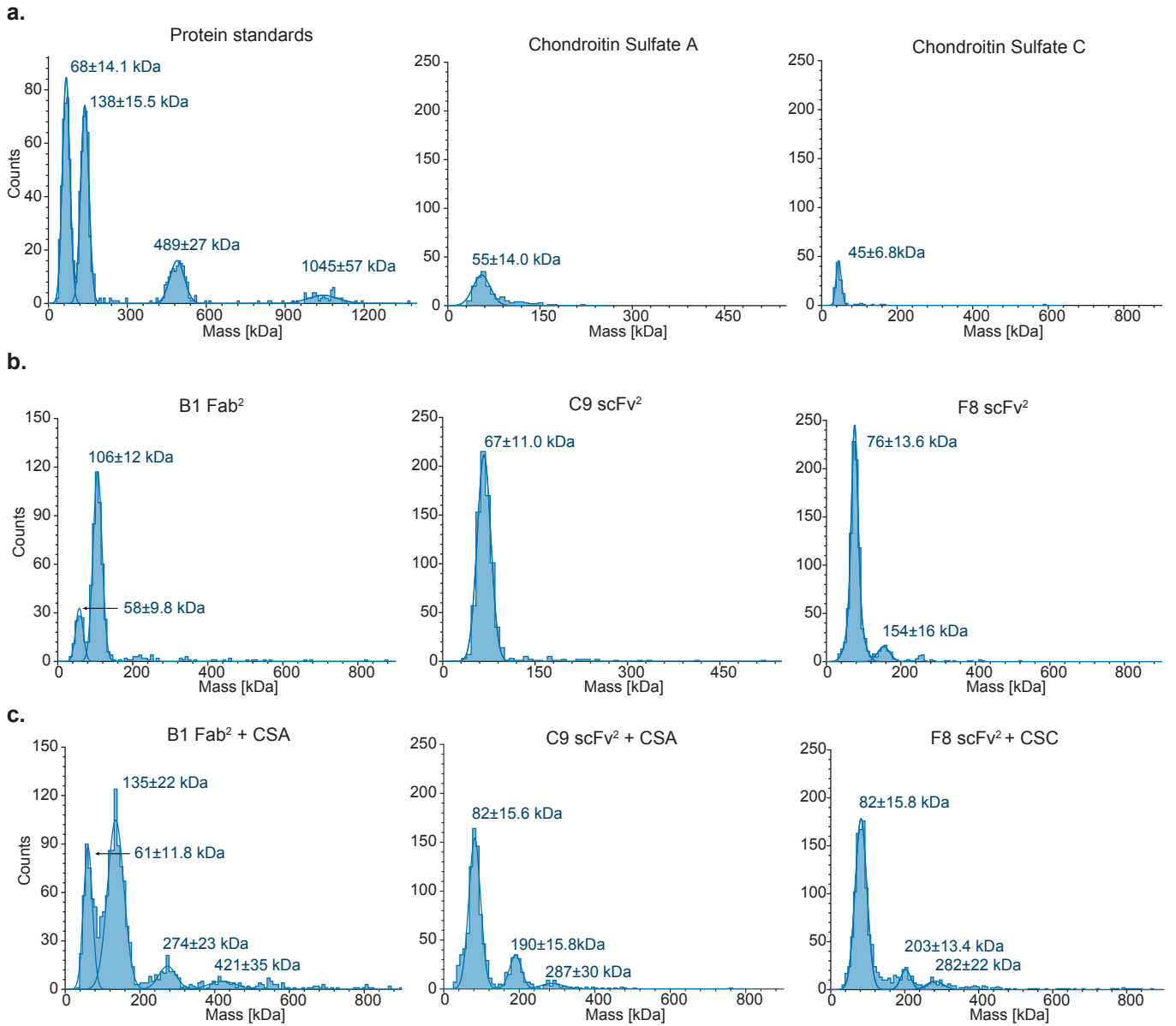
Chromatograms of HPLC-CS disaccharide analysis of the different fractions (input, flow through and elution) of ofCS pull-downs by scFv² (F3, F11, F8 and C9) immobilized on a column. ofCS was digested with chABC while bound to the antibodies to fingerprint the binding pocket, compared to CS standards.

Supplementary Fig. 14: Full-chain analysis of ofCS pull downs by F8.



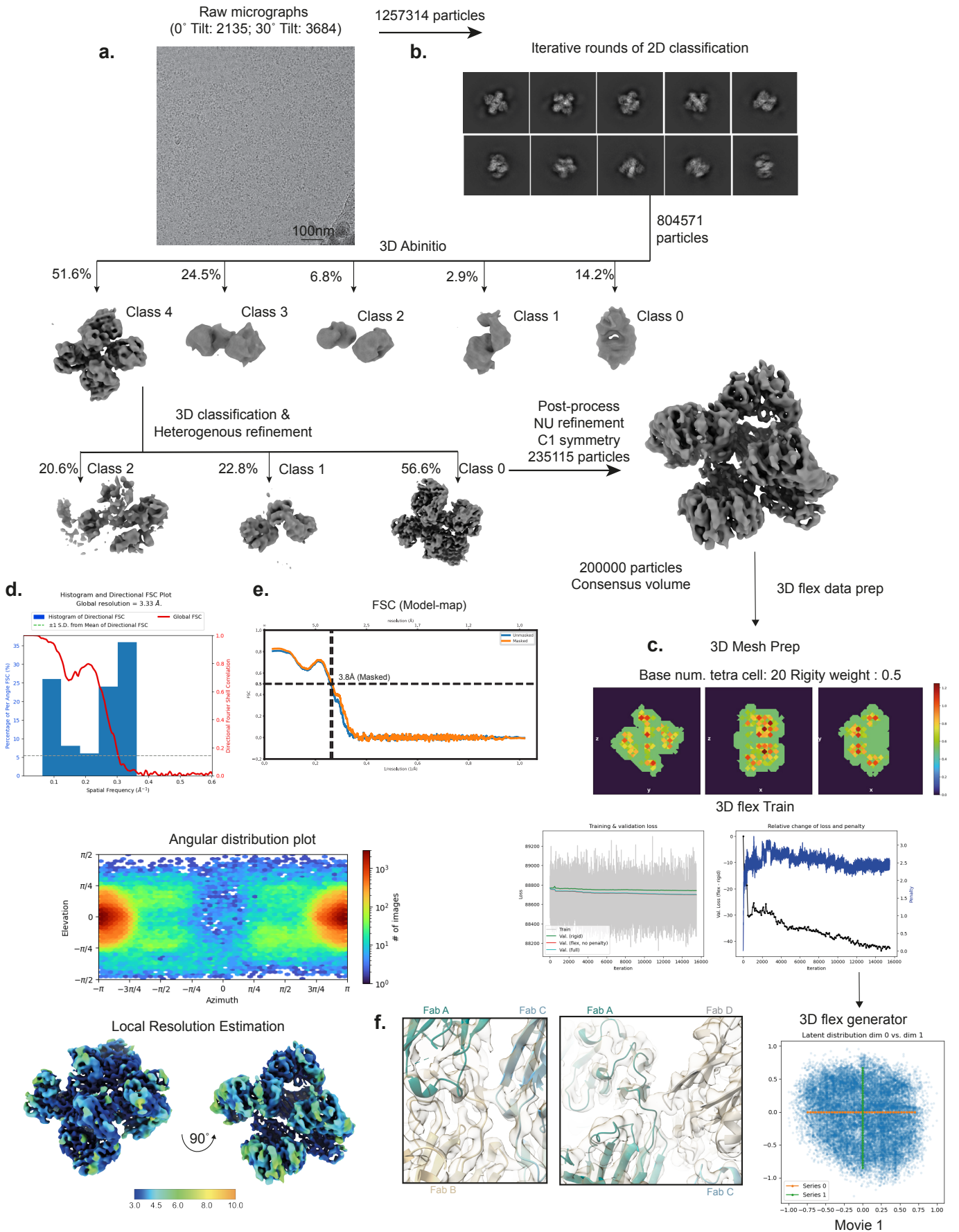
Chromatograms of HPLC-CS disaccharide analysis of the different fractions (input, flow through, wash and elution) of ofCS pull-downs by F8 scFv² immobilized on a column, compared to CS standards.

Supplementary Fig. 15: B1, C9 and F8 antibody fragments oligomerize along CS chains.



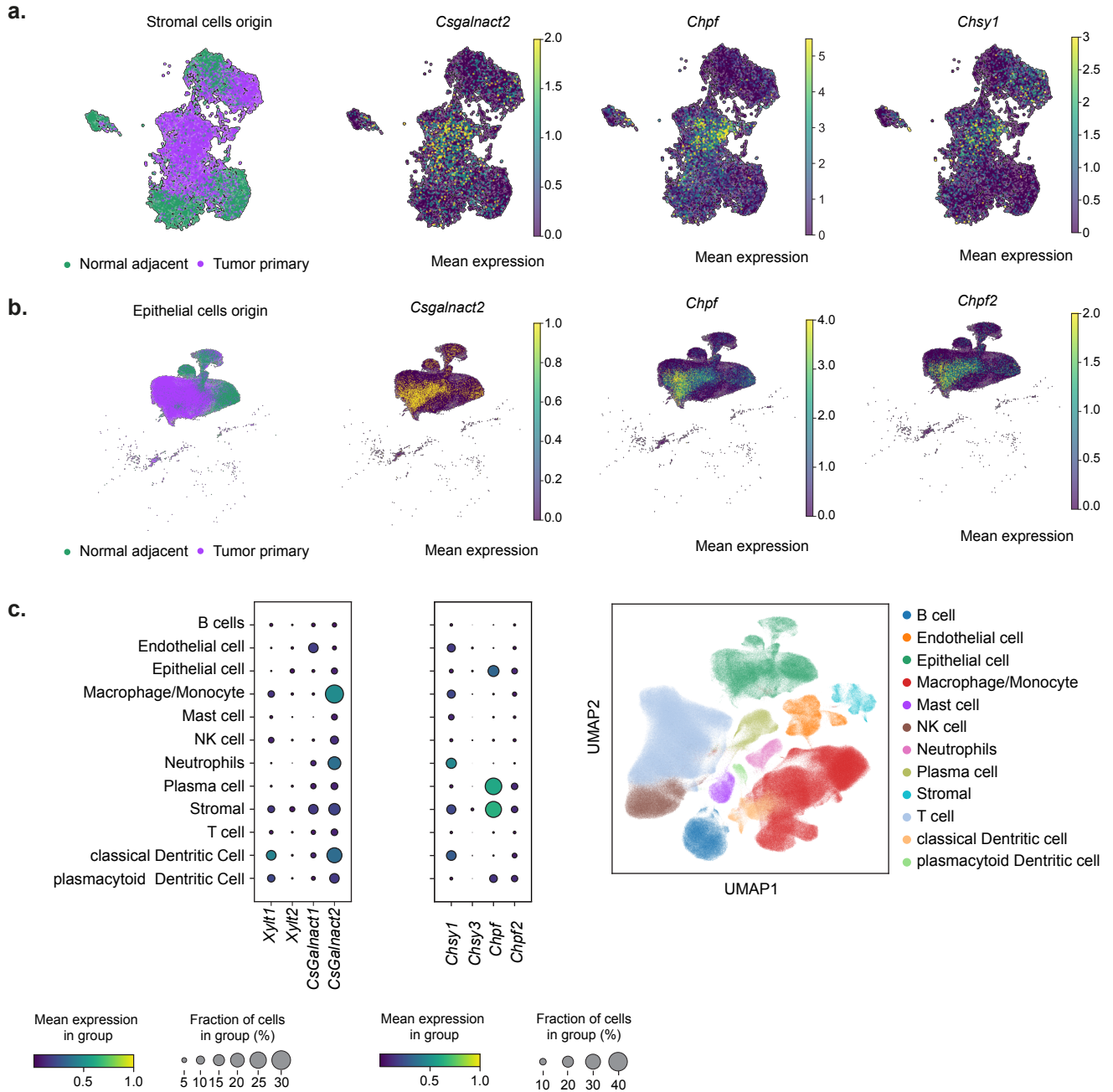
a. Mass photometry contrasts of protein standards, soluble chondroitin sulfate A and C, **b.** dimerized antibody fragments (B1 Fab², C9 scFv² and F8 scFv²), and **c.** antibody:CS complexes (B1 Fab² +/- CSA, C9 scFv² +/- CSA, F8 scFv² +/- CSC).

Supplementary Fig. 16: Workflow for structural analysis of B1:CSA complexes.



a. Representative micrograph of B1:CSA complex. **b.** Cryo-EM data processing workflow: reference free 2D classification followed by Ab-initio and heterogenous refinement. Non-Uniform refinement on the best class with C1 symmetry. **c.** 3D flex data workflow: Input particles and map prep job followed by Mesh preparation with 0.5 rigidity. 3D flex training was performed with 2 latent dimensions and the flex model was used to generate conformational movements by 3D flex generator job. **d.** 3dFSC plot showing the global resolution calculated as 3.3Å at FSC 0.143, and the angular distribution plot from the final NU refine job. The final map is colored based on the local resolution estimation. **e.** Model - map FSC plot showing 3.8Å at FSC 0.5. **f.** Model fit into the final map at the Fab:Fab interface is shown at transparency 50%.

Supplementary Fig. 17: Tumor cells up-regulate CS-initiation and elongation factors in NSCLS cohort.

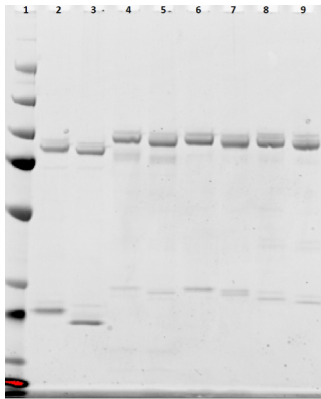


a. UMAP visualization of integrated non-small cell lung cancer (NSCLC) single-cell RNAseq transcriptome data for the expression of selected genes involved in the CS-initiation (*Csgalnact2*) and elongation (*Chpf*, *Chsy*) for stromal and **b.** Epithelial cells origin. **c.** Left panel: Dot plot expression analysis of genes involved in the CS-initiation (*Xylt1*, *Xylt2*, *Csgalnact1*, *Csgalnact2*) and elongation (*Chsy1*, *Chsy3*, *Chpf*, *Chpf2*), in distinguished cell types. Dot sizes refer to the fraction of cells expressing the gene. Right panel: UMAP visualization of the single-cell NSCLC dataset colored by cell type (as defined by cell annotation).

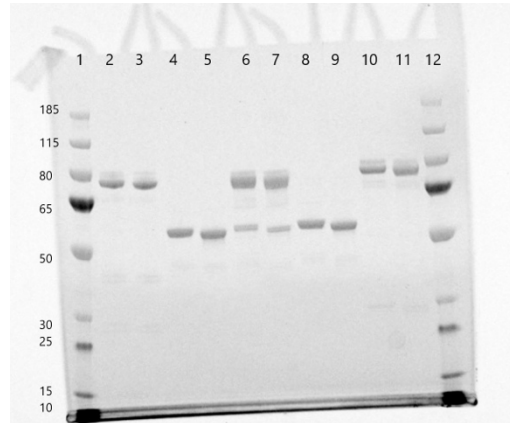
Supplementary Figure 18: Uncropped scans of blots used through the Supplementary File

a. Blots used in Supplementary Fig. 2a

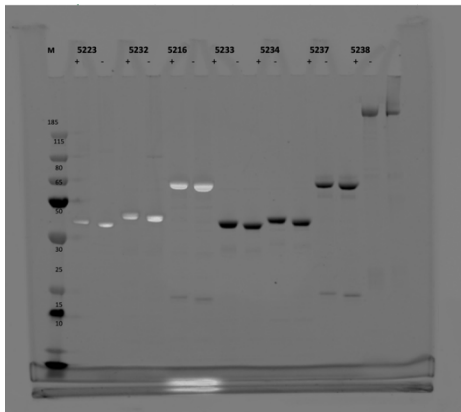
Lanes 2 and 3: B1 Fab²



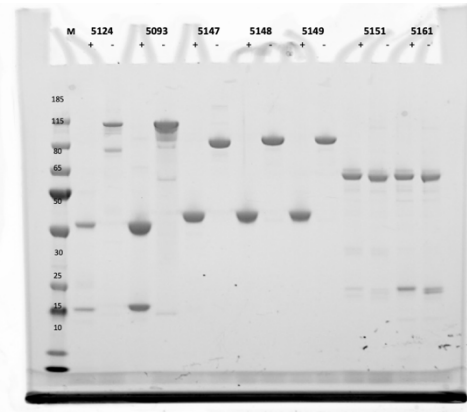
Lanes 10 and 11: F3 scFv²



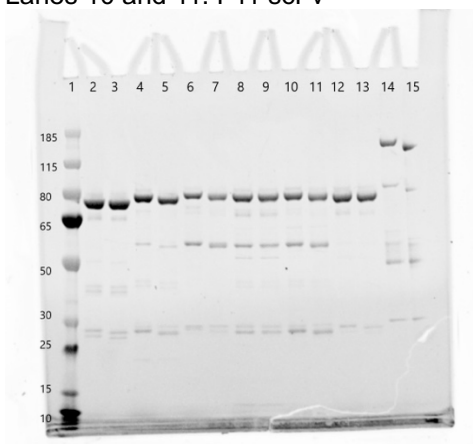
Samples 5237: C9 scFv²



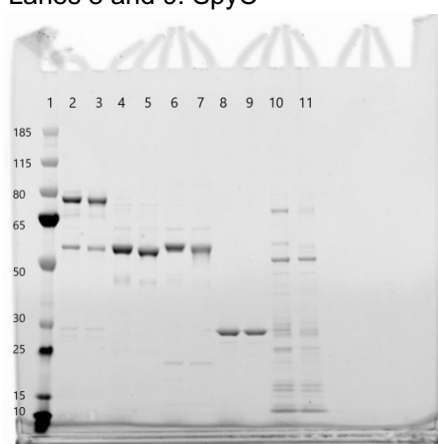
Samples 5151: F8 scFv²



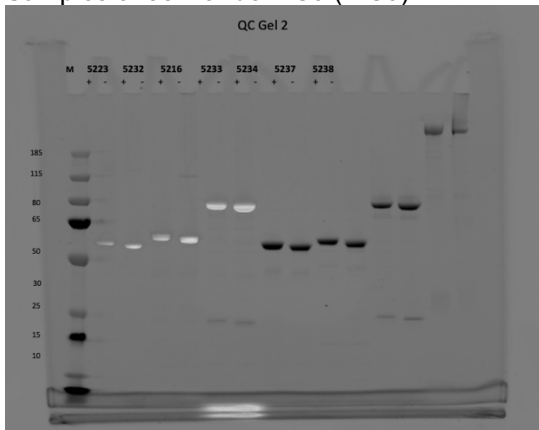
Lanes 6 and 7: F4 scFv²
Lanes 10 and 11: F11 scFv²



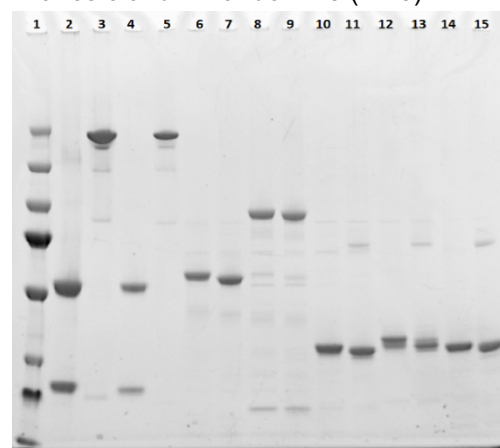
Lanes 2 and 3: B3 scFv²
Lanes 8 and 9: SpyC²



Samples 5233: Tandem C9 (T-C9)



Lanes 6 and 7: Tandem F3 (T-F3)

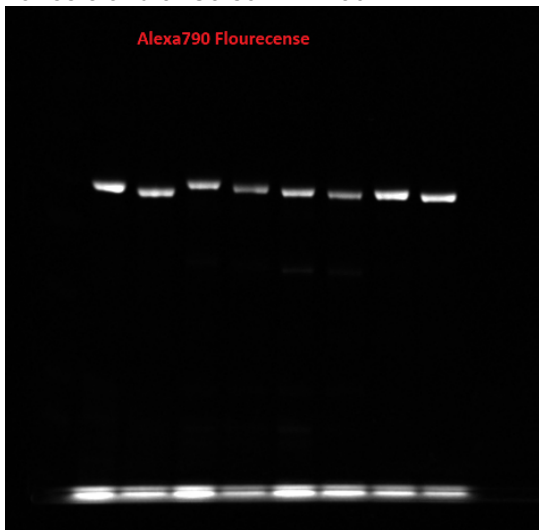


b. Blots used in Supplementary Fig. 9f

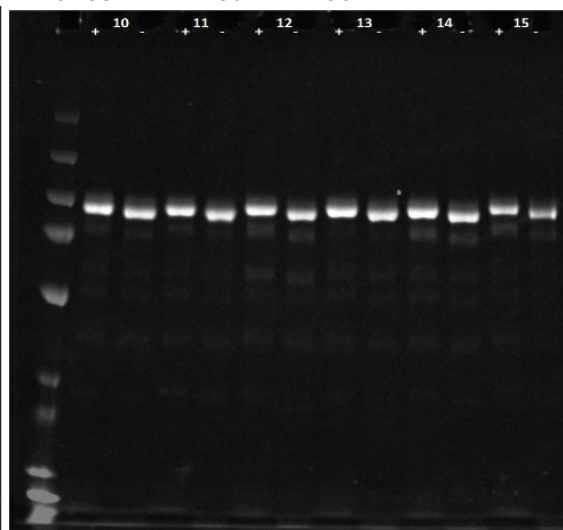
Fluorescence scans

Lanes 4 and 5: F4 scFv²-A750

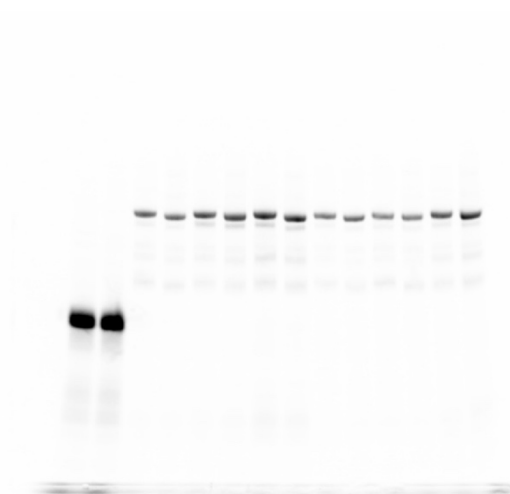
Lanes 8 and 9: C9 scFv²-A750



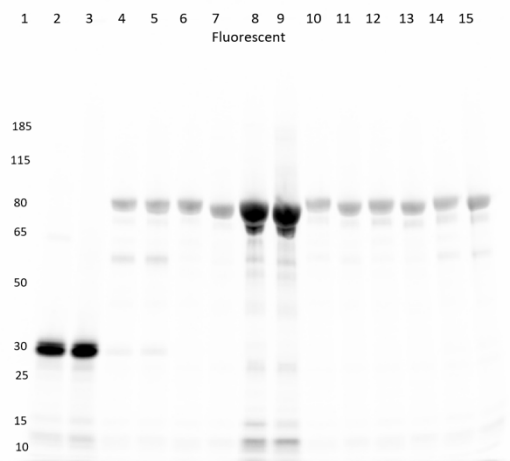
Lanes 14: F11 scFv²-A750



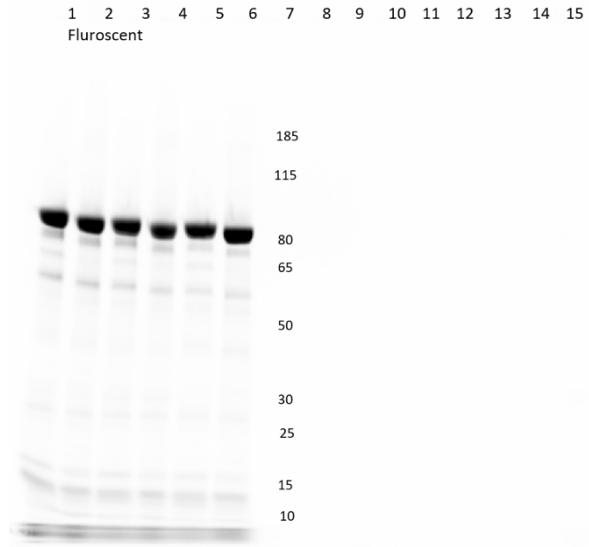
Lanes 3 and 4: F8 scFv²-A750



Lanes 2 and 3: SpyC2-A750
Lanes 8 and 9: F3 scFv²-A750

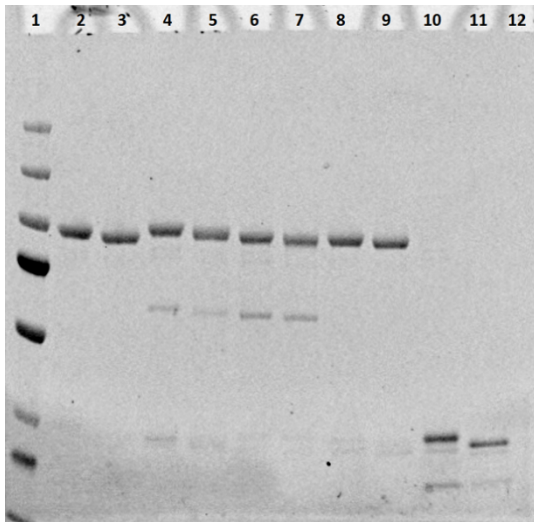


Lanes 3 and 4: B3 scFv²-Alexa750

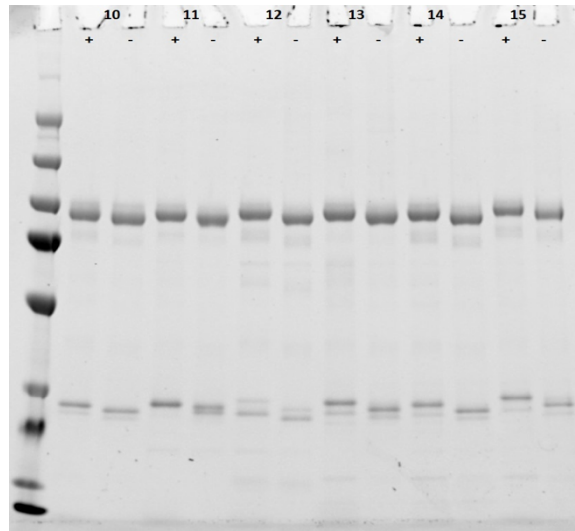


UV/Vis scans

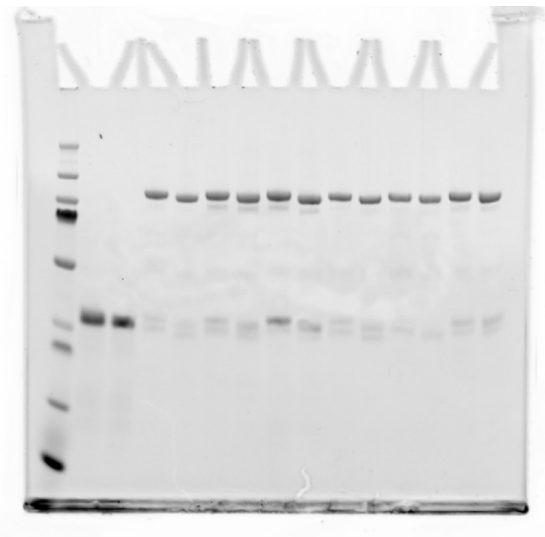
Lanes 4 and 5: F4 scFv²-A750
Lanes 8 and 9: C9 scFv²-A750



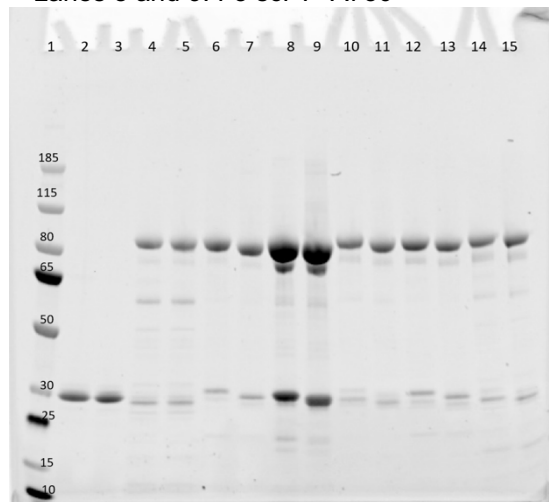
Lanes 14: F11 scFv²-A750



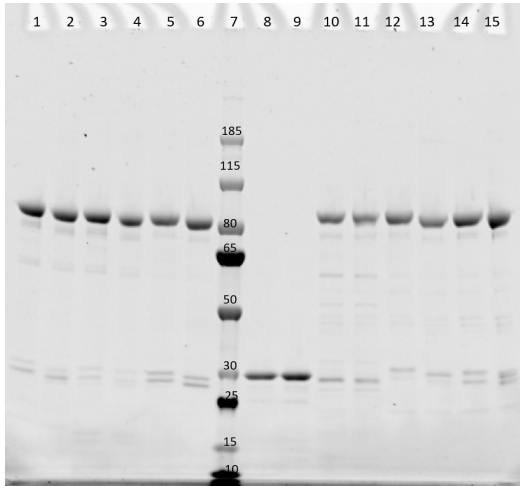
Lanes 3 and 4: F8 scFv²-A750



Lanes 2 and 3: SpyC²-A750
Lanes 8 and 9: F3 scFv²-A750



Lanes 3 and 4: B3 scFv²-A750

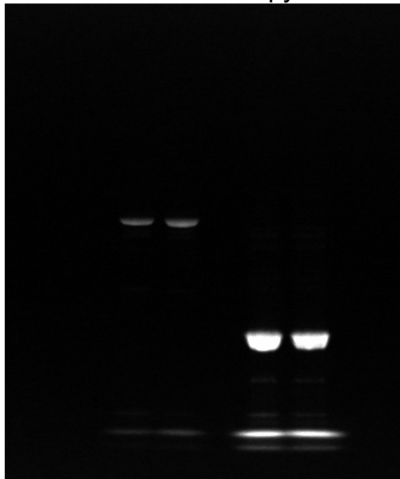


c. Blots used in Supplementary Fig. 9h

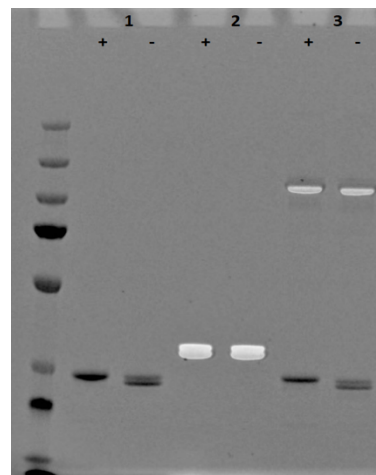
Fluorescence scans

Lanes 1 and 2: ABD-C9-scFv²-A750

Lanes 3 and 4: ABD-SpyC²-A750



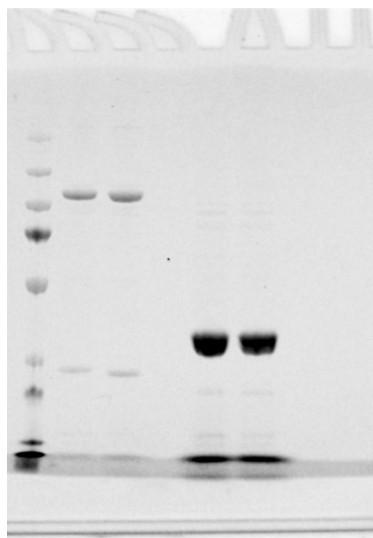
Lanes 3: ABD-F8-scFv²-A750



UV/Vis scans

Lanes 1 and 2: ABD-C9-scFv²-A750

Lanes 3 and 4: ABD-SpyC²-A750



SUPPLEMENTARY TABLES

Supplementary Table 1: List of hits obtained by Mass Spectrometry analysis of affinity enriched cancer cell supernatant, including gene, identifier, protein names and location.

Gene	Identifier	Protein	Location
SULF2	Q8IWU5-2	Extracellular sulfatase-2	Cell surface
LAMC2	Q13753	Laminin subunit gamma-2	Secreted, ECM, Basement membrane
TGFBR3	Q03167	Testican-3	Secreted, ECM, Cell membrane
SRPX	P78539-4	Sushi repeat containing protein	Cell surface
APLP2	Q06481-3	Amyloid beta precursor like protein 2	Cell membrane, Nuclei
LAMB2	P55268	Laminin subunit beta-2	Secreted, Basement membrane
AGRN	O00468-6	Agrin	Secreted, ECM
COL12A1	D6RGG3	Collage type XII alpha 1 chain	ECM
SDC4	P31431-2	Syndecan-4	Cell membrane, Secreted,
HSPG2	P98160	Heparan sulfate proteoglycan 2	Secreted, ECM, basement membrane
ITGB1	P05556	Integrin beta-1	Cell membrane
BGN	P21810	Biglycan	Secreted, ECM
CD44	P16070	CD44	Cell membrane
CSF1	P09603	Macrophage colony-stimulating factor 1	Cell membrane
VCAN	E9PF17	Versican	Secreted ECM
LAMA4	A0A0A0MTC7	Laminin subunit alpha 4	ECM
CSPG4	Q6UVK1	Chondroitin sulfate proteoglycan-4	Cell membrane
DCN	P07585	Decorin	Secreted, ECM
SERPINI1	Q99574	Neuroserpin	Secreted
GPC4	O75487-2	Glypican-4	Cell membrane, Secreted
CCBE1	Q6UXH8	Collagen and calcium binding EGF domain containing protein 1	Secreted
GPC1	P35052	Glypican-1	Cell membrane, secreted

Supplementary Table 2: List of cells used across the study including cell line name, cell type, origin, disease, and accession number (Cellosaurus ID)

Cell lines	Type	Origin	Disease	Cellosaurus ID
A375	Epithelial	Human	Malignant melanoma	CRL-1619
A549	Epithelial	Human	Lung carcinoma	CCL185
Colo205	Epithelial	Human	Colorectal adenocarcinoma	CCL-222
CT26	Epithelial	Mouse	Colon carcinoma	CRL-2638
HT29	Epithelial	Human	Colon adenocarcinoma	HTB-38
MiaPaca2	Epithelial	Human	Carcinoma	CRL-1420
PC-3	Epithelial	Human	Prostate adenocarcinoma Grade IV	CRL-1435
SkBR3	Epithelial	Human	Adenocarcinoma	HTB-30
SW480	Epithelial	Human	Adenocarcinoma colorectal, dukes type B	CCL-228
4T1	Epithelial	Mouse	Mimics human breast cancer, stage IV	CRL-2539
Karpas299	Hematological	Human	Lymphoma non-Hodgkin	CVCL_1324
KG-1	Hematological	Human	Acute myelogenous leukemia	CCL-246
Myla2059	Hematological	Human	T-cell non-Hodgkin lymphoma	CVCL_5342
NALM6	Hematological	Human	Acute lymphoblastic leukemia (ALL)	CRL-3273
REH	Hematological	Human	Acute lymphocytic leukemia (non T, non B)	CRL-8286
697	Hematological	Human	Childhood B acute lymphoblastic leukemia	CNCL_0079
MG63	Mesenchymal	Human	Osteosarcoma	CRL-1427
MNNG	Mesenchymal	Human	Osteosarcoma	CRL-1547
TC-71	Mesenchymal	Human	Ewing Sarcoma	CVVL_223
U2OS	Mesenchymal	Human	Osteosarcoma	HTB-96
U87mg	Mesenchymal	Human	Glioblastoma	HTB-14

Supplementary Table 3: List of human tissue micro-arrays (TMA) used across the study including name, type of array, link to vendor and use in the study.

Name	Type of array	Link to vendor	Use in the study
BR1921c	Breast carcinoma with adjacent and normal tissues	https://www.biocomax.us/tissue-arrays/Breast/BR1921c	<ul style="list-style-type: none"> - Fig. 2b: Breast tissue stained with C9 (A7, F12) and F8 (A7, F12) - Fig. 2d: Breast arrays signal quantifications (C9 and F8) - Supplementary Fig. 3a
CO702d	Colon primary cancer with metastatic cancer and normal tissues	https://www.biocomax.us/tissue-arrays/Distant_Metastasis/CO702d	<ul style="list-style-type: none"> - Fig. 2b: Scans of colon tissue stained with C9 (B2, G1) and F8 (B8, G1) - Fig. 2d: Colon arrays signal quantifications (C9 and F8) - Supplementary Fig. 3b
DGS2081	Digestive system array (including benign, malignant, adjacent, and normal tissues)	https://www.biocomax.us/tissue-arrays/Multiple_Organ_Tumor/DGS2081	<ul style="list-style-type: none"> - Fig. 2b: Scans of stomach tissues stained with C9 (D8, M6) and F8 (C4, M6) - Fig. 2b: Scans of esophagus tissues stained with C9 (A2, M1) and F8 (B5, M2) - Fig. 2d: Digestive system arrays signal quantifications (C9 and F8) - Supplementary Fig. 3c - Supplementary Fig. 7c
GL2083	Brain cancer with adjacent and normal brain tissues	https://www.tissuarray.com/tissue-arrays/Brain/GL2083c	<ul style="list-style-type: none"> - Supplementary Fig. 4a - Supplementary Fig. 7b: Scans of healthy brain stained with C9 and F8 scFv²
LC243a	Lung cancer and normal lung tissues	https://www.biocomax.us/tissue-arrays/Lung/LC243a	<ul style="list-style-type: none"> - Fig. 2b: Scans of lung tissues stained with C9 scFv² (A2, D2) - Supplementary Fig. 4b
LC1201b	Lung cancer with metastatic, adjacent and normal tissues	https://www.biocomax.us/tissue-arrays/Lung/LC1201b	<ul style="list-style-type: none"> - Fig. 2b: Scans of lungs tissues stained with F8 scFv² (B7, J6) - Supplementary Fig. 4c
LC2085d	Lung cancer with adjacent and normal tissues	https://www.biocomax.us/tissue-arrays/Lung/LC2085d	<ul style="list-style-type: none"> - Fig. 2c: from top to bottom, left to right (J11, J11, I14, C11) - Fig. 2d: Lung arrays signal quantifications (C9 and F8) - Supplementary Fig. 4d
ME1002b	Malignant melanoma with adjacent and normal skin tissues	https://www.biocomax.us/tissue-arrays/Skin/ME1002b	<ul style="list-style-type: none"> - Fig. 2b: Scans of skin tissues stained with C9 (E2, J5) and F8 (F2, J4)

		arrays/Melano/ME1002b	<ul style="list-style-type: none"> - Fig. 2d: Skin arrays signal quantifications (C9 and F8) - Supplementary Fig. 5a
PA482	Pancreatic ductal adenocarcinoma (PDAC)	https://www.biomax.us/tissue-arrays/Pancreas/PA482	<ul style="list-style-type: none"> - Fig. 2b: Scans of pancreas tissue stained with C9 (D3, F4) - Supplementary Fig. 5b
PA804b	Pancreas cancer and normal tissues	https://www.biomax.us/PA804b	<ul style="list-style-type: none"> - Fig. 2b: Scans of pancreas tissue stained with F8 (A5, F4) - Fig. 2d: Pancreas arrays signal quantifications (C9 and F8) - Supplementary Fig. 5c
TE481a	Testis cancer with testis tissue array	https://www.tissue-arrays.com/Testis/TE481a	<ul style="list-style-type: none"> - Supplementary Fig. 7a - Supplementary Fig. 7b: Scans of healthy testis stained with C9 and F8.
TP241b	Top 4 types of cancer (colon, breast, prostate, lung) tissue array	https://www.tissue-arrays.com/Multiple_Organ_Tumor/TP241b	<ul style="list-style-type: none"> - Fig. 2a - Supplementary Fig. 6a: Colorectal adenocarcinoma (A2), Breast Invasive ductal carcinoma (B3), Lung Squamous cell carcinoma (C3).

Supplementary methods

Phage display generation of antibody fragments binding ofCS

The phage display technology was utilized to generate human antibody fragments. Phage libraries were bio-panned over 3 to 4 rounds for successful enrichment of ofCS binders. Each round consisted of three main steps. Firstly, the panning step selects the positive binders to our antigen (ofCSG or ofCS) by incubating phages with ofCS-modified molecules. Next, the counter-panning step was employed to deplete low affinity and unspecific binders on a counter-antigen (PG or naked beads). Lastly, the selection step was performed either positively on an ofCS-carrying molecule or negatively on an ofCS-depleted molecule. At each round, potential binding candidates were eluted, amplified in *Escherichia coli* (*E. coli*), and tested over a succession of Polyclonal phage ELISA against ofCSPG and PG. The clones displaying the most promising binding properties were sequenced and further tested on Monoclonal phage ELISA to assess their binding to ofCSPG and PG.

The first strategy involved two libraries, namely the naïve LiAb-SFMAX™ (scFv) and the synthetic HuCAL (Fab)^{1,2} where ofCSPG and PG were used as antigens and counter-antigen, respectively. The counter-selection was carried out against HSPG (Sigma, #H4777) to deplete binders to negative charges. In this method, an additional competition ELISA was performed to further select clones sharing some epitope with VAR2CSA protein. The second strategy was run on the ALTHEA Gold semi-synthetic (scFv) library³, where purified ofCS was used for panning, and ofCSPG was used as the positive selection target.

Testing of rVAR2 binding to panning reagents

The presence of ofCS in the produced reagents was controlled by testing rVAR2 binding. The biotinylated-antigens were immobilized on Streptavidin-coated magnetic beads (SeraMag SpeedBeads, Sigma #2152104011150) at 3.4, 10, and 30 ng/μg of beads. After the beads were blocked, 0.1 μg/μl of V5 tagged-rVAR2 was added and incubated for 1h at room temperature. Bound rVAR2 was detected with anti V5-HRP antibody (Abcam, #ab1325). The reaction was activated with TMB-X-tra (Kementec, #4800) and stopped with 0.2M H₂SO₄. The signal was read on an ELISA reader at 450nm, plotted on GraphPad (Prism), and edited on Illustrator (Adobe).

Recombinant protein production

All proteins were produced using the following procedure. Synthetic DNA encoding proteins of interest were purchased from GeneArt (ThermoFisher). All constructs have NotI and NcoI restriction enzyme sites for cloning, a C-terminal 6xHistidine tag for purification, and when indicated additional N-terminal SpyTag and/or C-terminal V5 tag. The constructs were cloned into pET28 vector (Novagen) pre-digested with the same restriction enzymes, and plasmids from positive colonies were sequence verified (Eurofins). Variants of SpyC constructs were transformed into *Escherichia coli* (*E. coli*) BL21 DE3 (New England Biolabs, #C2527H) whereas antibody fragments and chABC (Uniprot P59807) constructs were transformed into *E. coli* Shuffle DE3 (New England Biolabs, # C3029J) for subsequent protein expression. Cells were grown in 2xYT media at 37°C until the early exponential phase where the temperature is decreased to 20°C followed by induction of protein expression with isopropyl β -D-1-thiogalactopyranoside (IPTG). After 16h induction, the cells were harvested and stored at -20°C. Cells were lysed in phosphate buffer and the soluble fraction was purified on HisTrap HP column (Cytiva #17524802). After reducing the conductivity the eluted material was purified using ion exchange chromatography. All SpyCatcher variants were purified using the anion exchange column HiTrap Q HP (HP, Cytiva #17115301) while the antibody fragments were purified using cation exchange column HiTrap SP HP (Cytiva #17115201) where they were eluted with a linear gradient of NaCl. chABC enzyme was purified using the size exclusion column Sephacryl S-300 HR (Cytiva #17059910). When indicated the albumin binding domain ABD035 was genetically fused to the N-terminus of the SpyC protein to increase the plasma half-life as previously described⁴.

Murine SpyCatcher-anti CD3 was produced as in⁵.

Antibody fragments conjugation to SpyCatcher variants

The SpyCatcher (SpyC)-Spy Tag (SpyT) click interaction was employed for all conjugations. When combined, a spontaneous covalent iso-peptide bond forms between the lysine (SpyC) and an aspartate (SpyT)⁶. To ensure a consistent degree of labeling across antibody fragments, the SpyC protein was labeled prior to coupling the antibody fragments.

For *in vivo* IVIS imaging, SpyC or SpyC² was labeled with Succinimidyl Ester activated Alexa-750 (A750) fluorophore (Invitrogen, #A20111). The mixture was incubated for 1h at room temperature and then added to a PBS pre-equilibrated 7kDa Zeba spin desalting column

(Thermo Fischer, #89878) to separate the free dye from the coupled protein, following the vendor's instructions. Protein concentration and degree of labeling were determined by measuring the absorbance on the Nanodrop (Thermo Fischer) at 280nm and 749nm following the manufacturer's instructions. The SpyC and SpyC² conjugations yielded a degree of labeling between 0.5 and 1.3 Alexa 750 per protein.

For Antibody-Drug-Conjugate (ADC) studies, SpyC protein with 2 cysteines genetically introduced was reduced with 3.5 molar excess of Tris(2-carboxyethyl) phosphine (TCEP) for 90 minutes at 37°C. Subsequently, a 3-molar excess of maleimide-valine-citrulline-MMAE linkers (Med Chem Express, #HY-15575) was added and incubated for 60min at room temperature. The free drug linker was removed with 7kDa Zeba spin column equilibrated in PBS. Protein concentration was calculated as previously and the drug:antibody ratio (DAR) was determined on the Nanodrop using the 280nm and 248nm ratio⁷.

For *in vitro* staining of cancer cells in blood, SpyC protein was mixed with 6-molar excess of Biotin-NHS (Sigma, #H1759) dissolved in dimethyl sulfoxide (DMSO), incubated for 1h at room temperature followed by biotin removal was removed using a Zeba spin column equilibrated in PBS.

Monomeric scFv or Fab were covalently dimerized with unmodified, A750 conjugated, MMAE conjugated, or biotinylated SpyC² in a 2.2:1 ratio for 1h at room temperature. Tandem scFv were conjugated with ABD-SpyC-A750 or ABD-SpyC-MMAE in a 1.2:1 ratio. The aCD3-T-C9 bispecific molecule was produced using a 1:1 molar ratio overnight with aCD3-SpyCatcher. All couplings were confirmed by sodium dodecyl-sulfate polyacrylamide gel electrophoresis (SDS-PAGE) to show successful conjugation of all SpyC proteins.

Semi-inactivation of C9-scFv-ADC

C9-scFv-ADC was prepared as described below by mixing ABD-C9-scFv with a free cysteine genetically introduced by incubating with 2.5 molar excess of maleimide-valine citrulline-MMAE linker, and removal of free drug linker. This ADC was subsequently reduced with 20 molar excess TCEP at 37°C for 60min. The generated free thiols were blocked with 20 molar excess of N-ethyl maleimide (NEM), and incubated for 60 min at room temperature. Subsequently, 20 molar excess of NHS-Acetate was added to block the free amines, for 60 min at RT. The inactivation chemicals were removed from the mixture by buffer exchanging into 1xPBS using 7kDa Zeba spin column equilibrated in PBS. The semi-inactivation of the ADC was confirmed by a significant reduction of its binding to commercialized ofCSPG (Aggrecan, Sigma) in ELISA, compared to the original ADC.

IF staining

Tissues were obtained, deparaffinized, and stained with the same procedure described in the main methods section “**Immunofluorescence staining of paraffin-embedded fixed tissues.**”. In the GAG inhibition IF experiment (**Supplementary Fig. 9e**), 25nM C9 scFv² was pre-incubated with 25 or 50 ug/ml of soluble CSA (Sigma #), or soluble HS (Ibex, #) for 15min before addition to the deparaffinized and blocked Karpas 299 tumor tissues, incubated 1h at RT and detected with 1:400 anti-V5 antibody (Invitrogen, #451098), before a succession of washes, nuclei staining with DAPI (Life Technologies, #D1306) and slide mounting. Tissues were scanned on Zeiss Axio Z1 automated slide scanner (20 X magnification, 0.8 NA objective), and image analysis on the ZEN lite software.

Flow binding on CAFs cell lines

CAFs cell lines were kindly shared by Chris D. Madsen, Lund University (Sweden). Human CAFs (vCAFs) were collected from patients following their consent protocol and immortalized using hTERT lentivirus as described by Gaggiolo *et al.*⁸. Mouse CAFs (mCAFs) were harvested from the mammary fat pad of MMTV-PyMT mice that developed breast carcinoma, as described by Calvo *et al.*⁹.

Cell lines were grown to reach 80% confluency, detached using Cell Stripper (Corning #25-056-CI), and counted for adding 100.000 cells /well resuspended in PBS with 2% FBS. Prior to staining, some wells were treated with 0.2mg/ml of chABC enzyme to control the CS specificity of binding. Next, 150nM of C9 or F8 scFv² were added to the cells and left to incubate 30min on ice, in duplicates. In a separate well, 1:300 diluted anti- α SMA antibody (Abcam, Cat#ab5694) was added as a positive control. The scFvs² were detected with 1:500 diluted anti-V5-FITC (Invitrogen, Cat#R963-25) while the anti- α SMA antibody was detected with 1: 500 Anti-Rabbit-Alexa647 (Thermo Fischer, Cat#A27040). Data were acquired on a Cytoflex 2 instrument (Beckman Coulter) and analyzed FlowJoTM (Becton Dickinson).

Pharmacokinetics (PK) study

Plasma sampling

Sprague Dawley male rats were purchased from Janvier at the age of 8-9 weeks and injected with 100 μ g of C9 scFv or ABD-C9 scFv protein at the age of 10 weeks. Blood samples were harvested after 2 minutes, 1, 5, 24, 48, 72 and 96 hours after injection. Blood samples were spun down 2000xg for 5 minutes and resulting supernatants were collected and spun again for

10 minutes at 2000xg. Plasma samples were diluted in 1xPBS to reach a 50% plasma concentration.

PK ELISA

An ELISA method was employed to assess the plasma concentration of injected proteins over time and calculate their half-lives. A 96 well-non-treated plate (ThermoFisher #R96025) was coated with 50 μ L per well of 3 μ g/ml anti-V5 antibody (Invitrogen, Cat#46-0705) diluted in 1xPBS and incubated overnight at 4°C. The coated plate was blocked with 150 μ L per well of PBS + 0.05% Tween 20 + 1% BSA (Sigma, #A3059) for 1h at 37°C on a shaker. After blocking, the plate was emptied, and plasma samples from injected mice were added to the plate at several dilutions (1:20, 1:40, 1:80, 1:160, 1:320). A standard curve was prepared with the injected proteins in 50% plasma binding buffer from [25-0.0004] μ g/ml concentration and added to the plate. Samples were incubated for 1h, 37°C on shaking. After three washes of PBS+0.05% Tween 20 (PBST), proteins were detected with 1:3000 anti-C-term His tag-HRP antibody (Miltenyi Biotec) for 1h, 37°C on shaking. Following three last washes with PBST, the plate was developed with TMB Plus 2 (Kementec, #4395), the reaction was stopped with 0.2 M H₂SO₄ and signals were read at 450 nm on an ELISA reader. Theoretical protein concentrations in plasma were interpolated from the standard curve and average concentrations from two individual rats were calculated and plotted using GraphPad (Prism).

Cytotoxicity assay

The toxicity of the ADC formulations was tested in various cell lines. 10,000 cells/well for Karpas; 2000 cells/well for A549 and MiaPaCa2; 1000 cells/well for MG63 and CT26 and 3000 cells/well for U87mg, A375 WT, A375 CHST11 KO and A375 B4GALT7 KO, were seeded in 96 well plates in RPMI1640 media (Gibco) with 5% FBS (Gibco) and 1% Penicillin/Streptomycin (P/S) (Thermo Fischer). Subsequently, cells were co-incubated with ADCs in different concentrations (600nM to 9pM), in triplicates for each experiment, at 37 °C with 5% CO₂ for 72h. Viable cells were measured using Cell Proliferation Kit II XTT (Roche, #11465015001) as per the manufacturers' instructions. Briefly, OD measurements at 450nm and 632nm using a multi-well spectrophotometer were used to estimate the percentage of viable cells. IC₅₀ values were determined by using a non-linear regression model (four parameters) in GraphPad (Prism) (Version 9.5.0).

Anti-CD3 binding ELISA

96-well plates (flat bottom MaxiSorp) were coated with 50µL of recombinant murine CD3 protein (ECD, hFc Tag, #50410-M02H) in the concentration of 0.1 mg/ml. Coated plates were left overnight at 4°C. The next day, plates were washed three times with washing buffer (PBS + 0,05% Tween 20) in a volume of 150µl per well. Subsequently, blocking buffer (PBS + 0,05% Tween 20 (Sigma Aldrich, #P7949) + 5% skimmed milk) was added in a volume of 150 µl per well. Following another washing step, five-fold dilutions of aCD3-T-C9, aCD3, and T-C9 (starting at 600nM) were prepared and added to the plates and left for 1-2 hours of incubation. Anti-His-HRP (Miltenyi Biotec) secondary antibody was used as the detection antibody and the plate was incubated for an hour at 37°C with gentle shaking. The plates were developed with the TMB-X buffer (Kementec, #4800A), stopped, and read as described in the "PK ELISA" section.

Flow binding on murine splenocytes

Spleens were freshly harvested from sacrificed BALB/c mice and disrupted through a cell strainer, washed in PBS2, and incubated at RT for 13mins in red blood cell lysis buffer containing 0.155 M ammonium chloride, 0.01 M potassium hydrogen carbonate, and 0.1 mM EDTAC. Cells were washed in PBS2 and incubated with [9.3-300] nM proteins (T-C9-aCD3, aCD3, and T-C9) for 30 minutes. After another wash with PBS2, cells were incubated with 1:500 anti-V5-FITC (Invitrogen, #R963-25) for detecting C9 constructs, 1:200 anti-penta-His-Alexa Fluor 488 (Qiagen, #35310) for detecting aCD3, and CD3-PerCP/Cy5.5 antibody (Clone 17A2). Binding was analyzed on a BD Fortessa 3-laser analyzer (Becton Dickinson). Data were analyzed on FlowJo™ (Becton Dickinson) and plotted on GraphPad (Prism).

REFERENCES

1. Knappik, A. et al. Fully Synthetic Human Combinatorial Antibody Libraries (HuCAL) Based on Modular Consensus Frameworks and CDRs Randomized with Trinucleotides.
2. Prassler, J. et al. HuCAL PLATINUM, a Synthetic Fab Library Optimized for Sequence Diversity and Superior Performance in Mammalian Expression Systems. *Journal of Molecular Biology* **413**, 261–278 (2011).

3. Valadon, P. *et al.* ALTHEA Gold LibrariesTM: antibody libraries for therapeutic antibody discovery. *mAbs* **11**, 516–531 (2019).
4. Zorzi, A., Linciano, S. & Angelini, A. Non-covalent albumin-binding ligands for extending the circulating half-life of small biotherapeutics. *Medchemcomm* **10**, 1068–1081 (2019).
5. Skeltved, N. *et al.* Bispecific T cell-engager targeting oncofetal chondroitin sulfate induces complete tumor regression and protective immune memory in mice. *J Exp Clin Cancer Res* **42**, 106 (2023).
6. Zakeri, B. *et al.* Peptide tag forming a rapid covalent bond to a protein, through engineering a bacterial adhesin. *Proc. Natl. Acad. Sci. U.S.A.* **109**, (2012).
7. Hamblett, K. J. *et al.* Effects of Drug Loading on the Antitumor Activity of a Monoclonal Antibody Drug Conjugate. *Clinical Cancer Research* **10**, 7063–7070 (2004).
8. Gaggioli, C. *et al.* Fibroblast-led collective invasion of carcinoma cells with differing roles for RhoGTPases in leading and following cells. *Nat Cell Biol* **9**, 1392–1400 (2007).
9. Calvo, F. *et al.* Mechanotransduction and YAP-dependent matrix remodelling is required for the generation and maintenance of cancer-associated fibroblasts. *Nat Cell Biol* **15**, 637–646 (2013).